UNIVERSITY OF LEEDS

This is a repository copy of *Comparison of oral tribological performance of proteinaceous microgel systems with protein-polysaccharide combinations*.

White Rose Research Online URL for this paper:
https://eprints.whiterose.ac.uk/184768/

Version: Accepted Version

**Article:**

Soltanahmadi, S orcid.org/0000-0002-6909-4776, Murray, BS orcid.org/0000-0002-6493-1547 and Sarkar, A orcid.org/0000-0003-1742-2122 (2022) Comparison of oral tribological performance of proteinaceous microgel systems with protein-polysaccharide combinations. Food Hydrocolloids. ISSN 0268-005X

https://doi.org/10.1016/j.foodhyd.2022.107660

© 2022 Elsevier Ltd. All rights reserved. This is an author produced version of an article, published in Food Hydrocolloids. Uploaded in accordance with the publisher's self-archiving policy.

**Reuse**

This article is distributed under the terms of the Creative Commons Attribution-NonCommercial-NoDerivs (CC BY-NC-ND) licence. This licence only allows you to download this work and share it with others as long as you credit the authors, but you can't change the article in any way or use it commercially. More information and the full terms of the licence here: https://creativecommons.org/licenses/

**Takedown**

If you consider content in White Rose Research Online to be in breach of UK law, please notify us by emailing eprints@whiterose.ac.uk including the URL of the record and the reason for the withdrawal request.

White Rose
university consortium
Universities of Leeds, Sheffield & York

eprints@whiterose.ac.uk
https://eprints.whiterose.ac.uk/

# Comparison of oral tribological performance of proteinaceous microgel systems with protein-polysaccharide combinations

Siavash Soltanahmadi, Brent S. Murray, Anwesha Sarkar*

Food Colloids and Bioprocessing Group, School of Food Science and Nutrition,
University of Leeds, UK

*Corresponding author:
Prof. Anwesha Sarkar
Food Colloids and Processing Group,
School of Food Science and Nutrition, University of Leeds, Leeds LS2 9JT, UK.
E-mail address: A.Sarkar@leeds.ac.uk (A. Sarkar).

## Graphical Abstract

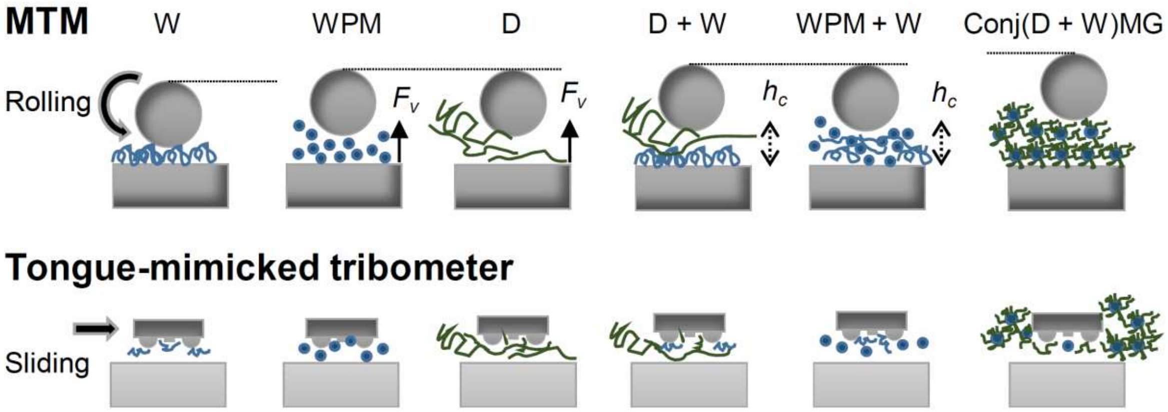

## Highlights

- Whey protein microgels (WPM) provide fluid-film and boundary lubricity
- WPM (41.7 vol%) deliver the same thickening behaviour as dextran (D) at 5 wt%
- WPM can be used as replacer for thickeners and lubrication-enhancer, simultaneously
- Microgels of D-conjugated whey protein deliver superlubricity upon entrained
- Superlubricity of conjugated microgels disappeared in a tongue-mimicked tribometer

# Abstract

Polysaccharides are often used as rheology modifiers in multiphasic protein-rich food systems. Recently, proteinaceous microgels have garnered research attention as promising lubricating agents. However, whether proteinaceous microgels can be used to replace polysaccharides in a tribological context remains poorly understood. In this study we compared the flow and oral-tribological behaviour of Newtonian solutions of the polysaccharide dextran (D, 1-11 wt%) when combined with a dispersion of whey protein isolate (W, 1-13 wt%) or whey protein microgel (WPM, 41.7 vol%) and compared with microgels of D-conjugated to W (Conj(D[11] + W[5])MG) or dispersions of WPM in W solutions. W and WPM alleviated frictional forces between elastomeric surfaces as well as biomimetic tongue-like surfaces in the boundary lubrication regime. Despite the negligible influence of D on the thin-film lubricity, its impact on viscous-facilitated lubricity was significant. The importance of measurements with the tongue-mimicked setup emerged where Conj(D[11] + W[5])MG did not show significant lubricity enhancement despite its outstanding performance with conventional tribo-testing setups. By optimising a combination of WPM and non-microgelled W, we demonstrate that a combined viscous and thin-film lubricity could be achieved through a single-protein-component without the need of polysaccharides. The dispersions of WPM (41.7 vol%) deliver the same flow and viscous-friction behaviour to that of 5 wt% D and excel in thin-film lubricity. These findings pave the way towards design of processed foods with clean labels, taking advantage of using a single proteinaceous moiety whilst delivering enhanced lubricity and viscosity modification without the need of any additional thickener.

**Keywords:** Oral tribology; Tongue-mimicked; Microgel; Polysaccharide, Protein-Polysaccharide; Viscosity; Lubrication; Conjugate

## 1. Introduction

Polysaccharides are widely used in the food industry, thanks to their non-toxic properties, accessibility and sustainability characteristics whilst imparting remarkable rheological properties that provide well-recognised favourable textural attributes (Yang, Li, Li, Sun, & Guo, 2020). Dextran (D) is a biocompatible, hydrophilic, neutral and branched food polysaccharide sourced from metabolites secreted from micro-organisms (Yang, 2020), and mainly composed of α(1→6) linkage with side chain branching (α (1→3)) attached to the backbone glucose units (Perrino, Lee, & Spencer, 2009). D also has broad applications in pharmaceutical products (e.g. as drug delivery vehicles) (Perrino, Lee, Choi, Maruyama, & Spencer, 2008) and has been subjected to tribological examinations when grafted onto surfaces as brushes, to mediate lubricity (Goren, Spencer, & Crockett, 2014; Perrino, 2008; Perrino, 2009; Rosenberg, Goren, Crockett, & Spencer, 2011).

Food proteins are extensively used to generate complex colloidal food systems possessing improved nutritional and structural functionality, including thickening and stabilization of emulsions (Araiza-Calahorra, Glover, Akhtar, & Sarkar, 2020; Sarkar, et al., 2016). Whey protein isolate (W), a food globular protein mainly composed of *β*-lactoglobulin (*β*-lg), *α*-lactalbumin (*α*-la) and bovine serum albumin, has been actively investigated in it's native, denatured or microgel form to enhance food product characteristics (Zembyla, et al., 2021). Microgels are particles ranging in size from a few tens of nm to a few tens of μm and consist of a fluid phase retained within a cross-linked network of macromolecules. Whey protein microgels (WPM) have shown exceptional ability as Pickering stabilizers of oil-in-water (O/W) emulsions that can also delay lipase digestion of such emulsions (Sarkar, 2016), act as fat replacers (Liu, Tian, Stieger, van der Linden, & van de Velde, 2016) and also as aqueous lubricants in orally relevant conditions (Andablo-Reyes, et al., 2019; Sarkar, Kanti, Gulotta, Murray, & Zhang, 2017). WPM are typically formed via heat-treatment of aqueous solutions of W (typically at ≥ 65 °C), resulting in internal cross-linking of the molecules via hydrogen bonding, hydrophobic interactions and disulfide bonding, under the appropriate conditions, to form the internal microgel biopolymer network (Araiza-Calahorra, 2020; Sarkar, 2017; Sarkar, 2016). While a thin-film adsorption-based mechanism, prompting *hydration* lubrication mechanism (Klein, 2013), has been proposed to explain the lubricity of W dispersions (Sarkar, Andablo-Reyes, Bryant, Dowson, & Neville, 2019; Zembyla, 2021), the lubricity of WPM was mainly attributed to a ball-bearing (or rolling) property of the entrained WPM particles into the contact interface (Liu, 2016; Sarkar, 2017).

Among other numerous efforts to improve the functionality of proteins, covalent conjugation of polysaccharide to proteins via the Maillard reaction has gained interest since it does not require any extraneous chemicals (Araiza-Calahorra, 2020; Sun, et al., 2011; Yang, 2020). Maillard conjugation has been used to boost protein properties in food applications, including enhanced resistance when subjected to environmental stresses (pH, ionic strength etc.), and improved protein solubility, stability (heat-induced aggregation etc.) and emulsifying properties (Araiza-Calahorra, 2020; Oliver, Melton, & Stanley, 2006). Conjugation is achieved simply by thermal treatment at an appropriate pH and appropriate water activity, leading to the condensation of the reducing end of the sugar in D with a deprotonated primary amino group of W, resulting in glycosylation (Araiza-Calahorra, 2020; Sun, Yu, Yang, , 2011).

Tribology has been proven to be a prominent tool to elucidate textural perception of food systems and to shed light on the links between sensory data and instrumental data (Pradal & Stokes, 2016; Sarkar, 2017; Sarkar & Krop, 2019; Sarkar, Soltanahmadi, Chen, & Stokes, 2021; Stokes, Boehm, & Baier, 2013). The mini traction machine (MTM2, PCS instruments, UK), as a bench-top instrument, has been extensively used to characterise the tribological performance of fluid/ semi-fluid/ solid substances particularly in oral-tribology investigations by means of providing the friction coefficient ($\mu$) data. Although the MTM2 has offered substantial insights into the tribology of food systems, it does not well represent the type of tribocontact conditions and materials involved in real mouth conditions. Recently, a method has been developed by Andablo-Reyes et al. (Andablo-Reyes, et al., 2020) which uses elastomeric surfaces mixed with a surfactant (Span 80) to create dome and pillar-shaped features that endow the contact surfaces with mechanical, wettability and surface texture characteristics much closer to that of the real tongue: the tongue-mimicked setup (Andablo-Reyes, 2020).

Although the tribological behaviour of suspensions of colloidal microgel systems and some food polysaccharides (pectin, xanthan, gellan, carrageenan and etc.) have been investigated in the literature (Andablo-Reyes, 2019; Sarkar, 2017; Stokes, Macakova, Chojnicka-Paszun, de Kruif, & de Jongh, 2011), no attempt has been made to understand the lubrication performance of polysaccharide-conjugated W, to the best of the authors' knowledge. Further, proteinaceous compounds have been suggested as fat-replacers but whether or not modified proteinaceous macromolecules (*e.g.* whey protein microgels) alone can be used to replace food polysaccharides in a tribological context remains unknown. The latter might be more difficult because of the complex non-Newtonian rheology of such polysaccharides - showing extreme shear-thinning behaviour, even at shear rates ($\dot{\gamma}$) above $10^5$ $s^{-1}$ (Stokes, 2011), which is of the order of $\dot{\gamma}$ that can occur between the tribological surfaces.

The aim of this study was to explore the capability of microgels to replace polysaccharide thickeners as lubricants in food systems. In order to assess that, we compared rheological and tribological properties of mixtures of D (at 5 wt%) + W with mixtures of WPM (at 41.7 vol%) + W at various comparable concentrations of W. Firstly, the influence of addition of D (1 - 11 wt%) to W (5 wt%) solution or WPM (41.7 vol%) dispersion on tribological and rheological behaviour of the mixtures is discussed and also compared to that of individual D, W or WPM solutions. Then, W-D conjugates and its microgelled version were investigated to explore whether such conjugation brings any novel lubricity features. D is a Newtonian polysaccharide and its conjugation to W has been well documented (Araiza-Calahorra, 2020; Sun, Yu, Yang, , 2011; Sun, Yu, Zeng, Yang, & Jia, 2011). Some of the results achieved by the conventional MTM2 tribological set up are critically assessed using the tongue-mimicked contact surfaces to understand the bio-relevance of this work to real oral processing.

## 2. Methods and materials

### 2.1 Materials

W powder (~90%) was supplied by Fonterra Limited (Auckland, New-Zealand). D (Molecular weight, $M_w$ = 500 kDa) and 4-(2-hydroxyethyl)-1-piperazineethanesulfonic acid (HEPES) were purchased from Fisher Scientific, UK and ITW Reagents, UK, respectively. Potassium bromide (KBr, >99%) and Sorbitan oleate (Span® 80) were purchased from Sigma-Aldrich, UK. Milli-Q water with a resistivity of 18.2 MΩ.cm at 25 °C (Millipore Corp., Bedford, UK) was used as the aqueous phase for preparation of the buffer and dispersions. Sodium azide (0.05 wt%) was employed as an antimicrobial agent. Ecoflex™ 00-30 (Smooth-On, USA) was purchased from Amazon, UK. The chemicals were used as received with no further purification.

## 2.2 Methods

A solution of 10 mM HEPES at pH 7.0 was used as a buffer solution for all dispersions except for W-D conjugate dispersions. For the latter, a higher ionic strength was required to compensate for a tendency for the pH to decrease during conjugation and hence a 50 mM HEPES buffer was used.

### *2.2.1 Preparation of WPM-containing dispersions*

A solution of 12.0 wt% W in 10 mM HEPES buffer (pH 7.0) was prepared at room temperature ensuring complete dissolution of the W. Corrections were made with reference to the actual protein concentration of the powder (~90%) in calculating the final concentration of W (*i.e.* 12 wt%). The solution was heat treated at 90 °C for 1 h using a water bath to promote crosslinking of the protein (Sarkar, 2017). The heat-set W gel (WPG) was cooled down for 15 min under running cold water and stored at 4 °C overnight. The WPG was broken down into macroscopic gel fragments using a hand blender (Bosch MSM6B150GB, UK; at 12500 rpm for 60 s) in 10 mM HEPES buffer (pH 7.0) with a weight ratio of 1.4:1 (HEPES:WPG). The dispersion of WPG fragments in HEPES solution was degassed (Intertronics, Thinky ARE-250) and passed twice through a custom made Jet Homogenizer (Jet Homogenizer, University of Leeds, UK (Sarkar, 2017)) operating at a pressure of 300 ± 20 bar (Sarkar, 2017). The dispersion of whey protein microgel particles in HEPES buffer after jet homogenization is referred to as WPM hereafter. The volume fraction of WPM in the dispersion was estimated as ~ 41.70% (Sarkar, 2017) from the initial mass (volume) of WPG and the volume of buffer in which it was dispersed. This assumed negligible swelling of the microgels upon dilution. For WPM + D and WPM + W samples, a pre-calculated amount of D or W was dissolved in the buffer just before shearing the WPG with the hand blender to obtain dispersions of WPM + D[1], WPM + D[5] and WPM + D[11] or WPM + W[1], WPM + W[3] and WPM + W[8]. The numbers 1, 5 and 11 in brackets indicate the [D] (wt%) in the total weight of the dispersions, respectively. Likewise the numbers 1, 3 and 8 in brackets denote the approximate [W] (wt%) in the total weight of the dispersions, respectively. The [W] (wt%) in HEPES buffer (*i.e.*, the free water; excluding the water trapped in the cross-linked network of WPM) are shown in Table S1, which were 1.06, 5.59 and 13.27 respectively. Since, D[5] and WPM (41.7 vol%) showed identical shear viscosity value ($\eta$) at $\dot{\gamma} = 2000$ s$^{-1}$ ($\eta_{2000}$) (see Results section), these two systems were ideal for comparison. A summary of naming and coding of all the samples prepared in this study is shown in Table 1.

**Table 1.** Sample nomenclature specifying the composition of the dispersions.

| Family of samples | Sample name | Dextran (wt%)‡ | Whey protein (wt%)‡ | Whey protein microgel (vol%)‡ |
|---|---|---|---|---|
| Biopolymer | D[1] | 1 | - | - |
| | D[5] | 5 | - | - |
| | D[11] | 11 | - | - |
| | W[5] | - | 5 | - |
| Biopolymer mixture | D[1] + W[5] | 1 | 5 | - |
| | D[5] + W[1]* | 5 | 1 | - |
| | D[5] + W[5]* | 5 | 5 | - |
| | D[5] + W[11]* | 5 | 11 | - |
| | D[11] + W[5] | 11 | 5 | - |
| Microgel + biopolymer mixture | WPM | - | - | 41.7 |
| | WPM + W[1]* | - | 0.62 | 41.7 |
| | WPM + W[3]* | - | 3.26 | 41.7 |
| | WPM + W[8]* | - | 7.74 | 41.7 |
| | WPM + D[1] | 1 | - | 41.7 |
| | WPM + D[5] | 5 | - | 41.7 |
| | WPM + D[11] | 11 | - | 41.7 |
| Conjugate | Conj(D[11] + W[5]) | 11 | 5 | - |
| Conjugate microgel | Conj(D[11] + W[5])MG | 11 | 5 | 41.7 |

‡ The values represent the concentrations of the relevant biopolymers (pristine or conjugated) in the total weight/ volume of the dispersions.

* The concentration of whey protein in free water (*i.e.* water content excluding WPM or D) can be found in Table S1.

### *2.2.2 Preparation of W-D conjugated dispersions*

Maillard conjugation was promoted via the method described by Araiza-Calahorra et al. (Araiza-Calahorra, 2020) with a slight modification. D and W (2:1 w/w) were mixed in 100 mL of Milli-Q water at room temperature. The pH of the mixture was adjusted to pH = 8.0 before freeze drying for at least 48 h. The freeze dried powder was placed in a humidity-controlled glass desiccator and incubated in an oven at 60 °C. The desiccator was preheated to 60 °C before introducing the powder. A relative humidity of ~80% was obtained using a saturated KBr solution. The powder was incubated for 48 h to induce the Maillard reaction (Araiza-Calahorra, 2020). The conjugated powders were stored in a dry desiccator before further use and analysis. The dispersion of W-D conjugate (that is, Conj(D[11] + W[5])) was prepared via dissolution of its powder in 50 mM HEPES to a [W] = 5 wt% (conjugated and non-conjugated) and [D] = 11 wt%. For the microgels of W-D conjugate, referred to as Conj(D[11] + W[5])MG, a conjugate solution equivalent to 10 wt% whey protein was prepared and thermally cross-linked at 65 °C for 1 h. The gel obtained was mixed with 50 mM HEPES at 1:1 w/w, fragmented with the hand blender followed by two passes through the Jet Homogenizer at 300 ± 20 bar. Conjugation influences the extent of protein unfolding and hence the subsequent gelation process (Sun, Yu, Yang, , 2011). In our case the temperature of 90 °C used to generate the WPG could not be used for gelation of the W-D conjugates because this temperature led to the formation of a very stiff gel that was too difficult to break down into microgel particles via the above methodology. Possibly this was due to the unconjugated dextran chains within the gel matrix acting as reinforcing fibres within the composite and enhanced rate of denaturation and aggregation of glycosylated protein chains, as compared to unconjugated protein (Sun, Yu, Yang, , 2011).

### *2.2.3 Preparation of non-microgelled dispersions*

The biopolymer solutions of dextran (D[1], D[5], D[11]), whey protein isolate (W[5]), and mixtures of dextran and whey protein (D[1] + W[5], D[5] + W[1], D[5] + W[5], D[5] + W[11], D[11] + W[5]) were produced by mixing the D and W at the concentrations denoted in brackets under magnetic stirring at room temperature (22 °C) at least for two hours until a homogenous dispersion was obtained.

### *2.2.4 Preparation of 3D-tongue-mimicking elastomeric surfaces*

The 3D-tongue-mimicking surfaces were developed based on previously published work (Andablo-Reyes, 2020). A code was developed using Matlab (MathWorks, USA) to randomly place 200 filiform-shaped cylindrical rods of 250 μm height and 175 μm radius, plus 20 fungiform-shaped hemispheres of 500 μm height and 500 μm radius on a unit cell of 1 cm$^2$, based on a spatial Poisson point distribution, defined by equation (1):

$$Pa(X = n) = \frac{\lambda^n e^{-\lambda}}{n!} \qquad (1)$$

where, *X* is the random variable representing the number of points in a defined area and $\lambda$ is the rate of the distribution reflecting the expected number of points in the area. This distribution informed the *x* and y coordinates for the fungiform and filiform ‘papillae’ on the master mould.

AutoCAD® (Autodesk, 2020, USA) was used to generate drawings of the above master mould of simulated papillae-containing surfaces. The AutoCAD drawing was 3D printed on an acrylic resin (Perfactory® HTM140) using a Perfactory 3D Printer (EnvisionTEC, Dearborn, USA) to produce a negative master mould. The 3D-tongue-mimicking surface was produced via a soft-lithographic process from the master mould. A solution of Ecoflex + 0.05 wt% Span 80 was degassed (Intertronics, Thinky ARE-250) and casted onto the polyvinyl alcohol(PVA)-treated master mould made of the acrylic resin (Perfactory® HTM140) (Andablo-Reyes, 2020). The solution was cured at room temperature for at least 5 h and the elastomeric replica (positive impression) was peeled off the mould. The replica was sonicated in isopropyl alcohol (IPA) and deionized water for 10 and 20 min, respectively, to remove traces of PVA and contamination before tribological testing. These soft elastomeric samples contained the random spatial distribution of filiform and fungiform papillae based on the characterization of size and distribution of papillae in a real human tongue mask (Andablo-Reyes, 2020).

### *2.2.5 Particle size measurements*

The hydrodynamic diameter ($d_H$) of the microgel particles was measured using a Zetasizer (Ultra Zetasizer, Malvern Panalytical) via dynamic light scattering (DLS) at 25 °C. The microgel-containing dispersions were diluted using HEPES buffer (pH 7.0) at a volume ratio of 1 : 99 (dispersion : HEPES) and dispersed in an ultrasonic bath at least for 15 min before measurements. Approximately, 1 mL of the diluted dispersion was pipetted into a polystyrene cuvette and scattered light detected at 173°. A refractive index of 1.54 for microgels and viscosity of $8.9 \times 10^{-4}$ Pa s (i.e., that of pure water) for aqueous medium were assumed. At least three replicates using three separate samples were conducted and the data were averaged (n = 3 × 3).

### *2.2.6 Bulk rheological measurements*

Rheological experiments were conducted using a modular compact rheometer (MCR - 302, Anton Paar, Austria). The $\eta$ was measured via cone-on-plate (CP50-1, angle 1°) geometry at 37 °C (to mimic oral physiological temperature). Viscosity results were measured at an initial value of $\dot{\gamma}$ = 1 $s^{-1}$, ramped logarithmically and terminated at 2000 $s^{-1}$ (i.e., increasing order of $\dot{\gamma}$). Five data points were recorded within each decade of the measurement range. At each $\dot{\gamma}$, a minimum 30 s window was set to achieve stress stability. The measurements were comprised of six steps. The samples were sonicated before measurements for at least 5 min, left stationery on the rheometer plate for 30 s before a pre-shear step at $\dot{\gamma}$ = 500 $s^{-1}$ for 120 s to hinder aggregation. Then the sample was left for 60 s to achieve a steady state immediately before the shear rate ramp. Lastly, to check for hysteresis, after the viscosity measurements a 120 s interval of steady state was applied and a viscosity measurement was taken at $\dot{\gamma}$ = 500 $s^{–1}$ immediately after. The hysteresis was negligible for all samples. Silicone oil, in combination with a thermo-control hood, was used to minimise the influence of evaporation during measurements. At least three replicates using separate samples were conducted and the data were averaged using OriginPro.

### *2.2.7 Tribological performance*

The frictional properties of the dispersions were investigated using two setups, namely a MTM2 and a modified rheometer (Kinexus Ultra+, Malvern Instruments, Malvern U.K.) enabling $\mu$ measurements using the afore-mentioned 3D-tongue-mimicked elastomer surfaces (Andablo-Reyes, 2020).

The tests with MTM2 were performed in a ball-on-disk configuration at 37 °C under a slide-to-roll ratio (SRR) of 0.5 and using smooth pristine polydimethylsiloxane (PDMS) specimens (ball of 19 mm and disc of 46 mm diameter). The PDMS specimens for MTM2 testing were supplied by PCS Instruments and had an elastic modulus and surface roughness ($S_a$) of 2.1 MPa and 20 nm respectively (Andablo-Reyes, 2019). The SRR was calculated using equation (2):

$$SRR = \frac{2(u_{a,X} - u_{b,X})}{u_{a,X} + u_{b,X}} \tag{2}$$

where, $u_{a,X}$ and $u_{b,X}$ are the speeds of body $a$ and $b$ in the $X$ direction (Sarkar, 2021). A load of 2 N was applied during experiments, corresponding to a Hertzian contact pressure of ~200 kPa (Sarkar, Andablo-Reyes, , 2019). The $\mu$ results are presented in the form of $\mu$ as a function of entrainment speed $(u)$ or the product of the limiting high-shear viscosity obtained at $\dot{\gamma} = 2000$ s$^{-1}$ (*i.e.* $\eta_{2000}$) and the $u$ (*i.e.* $\eta_{2000} \times u$), determined as described below (Sarkar, 2021). The friction forces were measured in order of increasing speed, at $10^{-3} < u < 2$ m s$^{-1}$. An extensive sample cleaning procedure was applied between each experiment to eliminate the influence of surface contamination which briefly included sonication steps in sodium dodecyl sulphate (2 wt% in DI water), IPA and DI water for 10 min at each step. At least three replicates using separate samples were conducted and the data were averaged.

Tribology of the samples were also tested using a biomimetic tongue surface emulating the stiffness, roughness and hydrophilicity of a real human tongue, the testing procedure is detailed previously (Andablo-Reyes, 2020). Briefly, a sample of the elastomer surface (i.e. Ecoflex™ 00-30 + 0.05 wt% Span 80, Young's modulus of 130 KPa - cut to 2 × 2 cm), which was 3D printed, was attached to the top plate of the rheometer with the centreline of the sample 1.5 cm from the centre of the top plate. A normal force of 1.0 N was applied to compress the sample against a stainless steel plate embedded in a pot filled with the dispersion. The pot was a custom-designed ring made from a UV-cured polymer. Tests were conducted at 37 °C in pure-sliding and unidirectional rotary tribocontact. Similar to tests with the MTM2, sliding was employed in the order from low ($5\times10^{-5}$ m $s^{-1}$) to high ($9\times10^{-3}$ m $s^{-1}$) $u$ values by increasing the angular velocity from 0.005 to 1 $s^{-1}$. For each sample a complete 2π rad rotation was applied at each velocity before a torque ($\tau$) was recorded. The $\tau$ was used to calculate the corresponding $\mu$ via equation (3):

$$\mu = \frac{\tau}{rF} \tag{3}$$

where, $F$ is the normal load (1 N) and $r$ is the radius of the top plate (0.025 m). Each dispersion was assessed by two readings on three separate elastomeric specimens and lubricant samples (n = 3 × 2).

### *2.2.8 Statistical analyses*

All measurements were done three times on triplicate samples prepared on separate days and are reported as the mean and standard deviation (n = 3 × 3) unless otherwise specified. The statistical analyses were conducted using one-way (ANOVA) and the significant difference between samples were considered when $p < 0.05$ using Tukey test.

# 3. Results and discussion

## 3.1 Size of WPM in different dispersions

The measured hydrodynamic sizes of the WPM particles in various dispersions are presented in Table 2. All samples showed monomodal size distributions (shown in Figure S1). Microgels showed polydispersity indices (obtained from correlation data via cumulants analysis) between 0.18 and 0.27 satisfying the analyses (Table 2). For non-conjugated dispersions (mixtures of WPM and D or W), the $d_H$ ranged between 94 ± 5 and 135 nm ± 2 (Table 2) assuming the microgels were spherical, justified by previous transmission electron microscopy (Sarkar, 2016). The size results for WPM particles are in agreement with the data previously reported for WPM particles produced under similar experimental conditions (Andablo-Reyes, 2019). Addition of W to WPM at different [W] did not influence the $d_H$ ($p > 0.05$) (Table 2). An increase of only 10 to 20 nm in the $d_H$ was observed upon presence of D in the process of microgel formation (Table 2).

Conjugation followed by microgel formation resulted in a significant change in microgel size. The remarkably larger size of Conj(D[11] + W[5])MG particles (Table 2) might be attributable to the lower protein-protein crosslinking density that is possible when W is conjugated to D (Sun, Yu, Yang, , 2011), resulting in a more open gel structure that might lead to greater swelling of the microgel particles when formed from the parent gel. On the other hand, the W-D conjugate gels have been shown to have elastic moduli of up to 5 times greater than that of the corresponding W gel (Araiza-Calahorra, 2020). As described earlier, this probably results from the higher concentration of biopolymers (dextran) within the gel matrix creating a composite gel with unconjugated D acting as reinforcing fibers. In addition to that, stiffer macrogels formed from W-D conjugates may be harder to break down to small microgel particles.

**Table 2.** Mean hydrodynamic diameter ($d_H$) and polydispersity index (PDI) of various whey protein microgel dispersions with or without the addition of biopolymers, measured at pH 7.0 and 25°C via *DLS*.

| **Sample** | **WPM** | **WPM + D[1]** | **WPM + D[5]** | **WPM + D[11]** | **Conj(D[11] + W[5])MG** | **WPM + W[1]** | **WPM + W[3]** | **WPM + W[8]** |
|---|---|---|---|---|---|---|---|---|
| $d_H$ (nm) | 115 ± $7^{a,c}$ | 124 ± $9^{a,c}$ | 125 ± $11^{a,c}$ | 135 ± $2^{a}$ | 227 ± $1^{b}$ | 115 ± $1^{a,c}$ | 94 ± $5^{c}$ | 99 ± $21^{a,c}$ |
| PDI | 0.234 ± 0.015 | 0.233 ± 0.005 | 0.236 ± 0.002 | 0.258 ± 0.006 | 0.185 ± 0.002 | 0.223 ± 0.001 | 0.267 ± 0.036 | 0.267 ± 0.036 |

## 3.2 Bulk rheological measurements

The $\eta$ of solutions of dextran (D[1], D[5], D[11]), WPM, W[5], W[5] mixtures with D[1] or D[5] or D[11], and Conj(D[11] + W[5]) are shown in Figure 1A. D is well-known to possess Newtonian properties (Carrasco, Chornet, Overend, & Costa, 1989; Sun, Yu, Yang, , 2011; Tirtaatmadja, Dunstan, & Boger, 2001) up to at least 30 wt% and $M_w$ of $2\times10^6$. Average $\eta$ values across the measured $\dot{\gamma}$ for D[1], D[5] and D[11] were 1.2, 9.9 and 38.2 mPa s respectively (Figure 1A). These are close to values of 1.52, 6.18 and 22.70 mPa s at 25 °C reported for dextran with a $M_w$ of $5.31\times10^5$ at concentrations of 1, 4.7 and 9.5 wt%, respectively (Carrasco, 1989). In general, the viscosities of dextran solutions are expected to increase with higher $M_w$ and concentration (Carrasco, 1989; Tirtaatmadja, 2001), corroborating our findings. Log $\eta$ versus log [D] (see Figure S2 in Supporting Information) showed a slope of 1.4, which is the same as reported by Tirtaatmadja et al. (Tirtaatmadja, 2001). This shows that D[11] (the highest concentration in this study) was below the critical overlap concentration (Yang, 2020), suggesting a random-coil branched configuration with long side-chains in its branches.

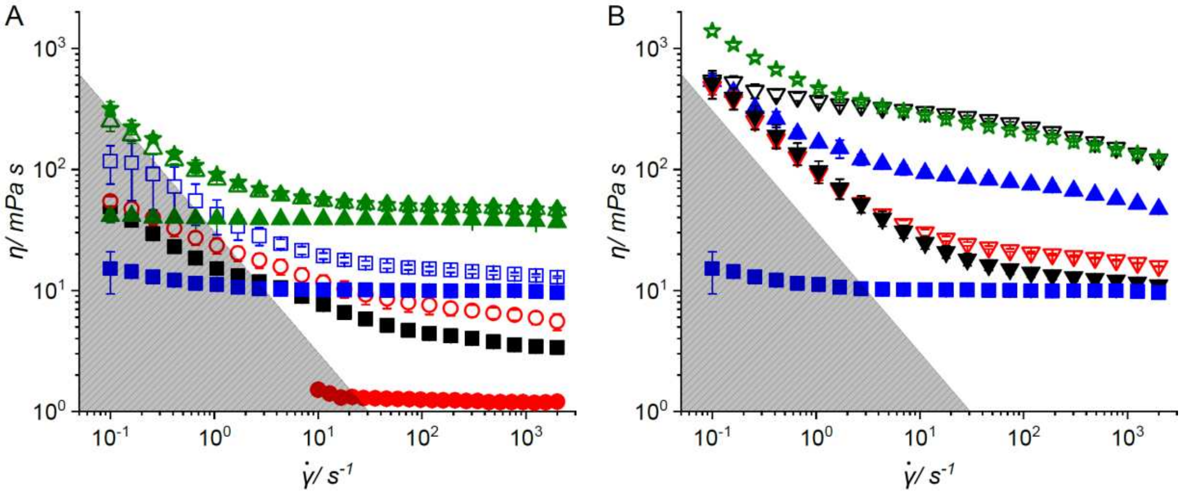

**Figure 1.** (A) Flow curves of the biopolymer solutions, *i.e.* dextran solutions D[1] (●), D[5] (■) and D[11] (▲); whey protein solution W[5] (■), mixtures of dextran and whey protein solutions D[1] + W[5] (○), D[5] + W[5] (□), D[11] + W[5] (△), and the conjugate Conj(D[11] + W[5]) (★). (B) Flow curves of the microgel systems WPM (▼), WPM + D[1] (▽), WPM + D[5] (▲), WPM + D[11] (▽), and the conjugated microgel Conj(D[11] + W[5])MG (☆), plus the D[5] (■), result from (A) is also shown for comparison. The shaded-hatch region in the curves denotes the invalid data range due to the geometrical limitations of the rheometer. Means are calculated based on readings on at least triplicate samples (n ≥ 3).

Whey protein solutions may show non-Newtonian behaviour (Rao, 2014) depending on the [W] and pH (Dissanayake, Ramchandran, & Vasiljevic, 2013), attributed to shear-induced rupture of inter-particle/molecular bonds or non-destructive alignment of the globular structure of whey protein with the flow direction. In our measurements, W[5] showed a moderate shear-thinning behaviour with $\eta$ dropping from 10.5 mPa s at $\dot{\gamma} = 4$ s$^{-1}$ to 3.4 mPa s at $\dot{\gamma} = 2000$ s$^{-1}$. The $\eta$ at $\dot{\gamma} = 2000$ s$^{-1}$ almost seemed to plateau (Figure 1A), indicating minimal protein-protein interactions occurring between W molecules. The limiting high-shear viscosity can be used to estimate the hydrodynamic forces in tribological studies (de Vicente, Stokes, & Spikes, 2005; Sarkar, 2021; Selway, Chan, & Stokes, 2017). The $\eta_{2000}$ values were used in this study to normalise $\mu - u$ plots to the influence of viscous forces (discussed later).

All mixtures of W[5] + D exhibited shear thinning in the lower values of $\dot{\gamma}$ with their $\eta$ appearing to level off at the highest $\dot{\gamma}$ values (Figure 1A). The addition of W slightly increased $\eta_{2000}$ of D[1] + W[5], D[5] + W[5] and D[11] + W[5] dispersions (5.5, 12.9 and 46.2 mPa s respectively) with their viscosities approaching to that of the corresponding D solutions alone, except for D[1] + W[5]. Increased [D] in solutions of D + W[5] shifted the onset of Newtonian behaviour to lower $\dot{\gamma}$ values (Figure 1A). The much larger molecular volume of D (Carrasco, 1989; Tirtaatmadja, 2001) means that D is expected to dominate the $\eta$ behviour, promote steric hindrance and disrupt inter-particle/molecular interactions between W molecules. Hence significant shear thinning only appears at lower $\dot{\gamma}$ in the mixtures, where there is more time for W molecules to rearrange and interact.  As it can be seen in Figure 1A, Conj(D[11] + W[5]) showed an identical shear-thinning behaviour to that of D[11] + W[5]. This is probably a result of the low degree of conjugation (< 20%) under the conditions used (Araiza-Calahorra, 2020) which essentially suggests the dominance of free D and W on the shear flow behaviour of Conj(D[11] + W[5]) dispersion.

Figure 1B presents $\eta$ of WPM, WPM + D[1], WPM + D[5], WPM + D[11], and Conj(D[11] + W[5])MG dispersions. The most intense shear-thinning behaviour was observed for WPM, showing an almost 50-fold decrease in $\eta$ across the measurement window, with $\eta_{2000} = 11$ mPa s. The high shear-thinning behaviour of WPM has been discussed elsewhere (Andablo-Reyes, 2019; Sarkar, 2017). We note that $\eta_{2000}$ of WPM was over three-times greater than that of W[5] (Figure 1B). The addition of D to WPM (WPM + D) significantly enhanced the resultant $\eta$ across the measured $\dot{\gamma}$

values, particularly at $\dot{\gamma}$ > 100 s$^{-1}$, which is caused by the existence of higher overall concentration of biopolymers in the dispersed phase. Among WPM + D dispersions, a high shear-rate plateau was achieved for WPM + D[1] displaying a $\eta_{2000} = 15.9$ mPa s. With increased [D], the shear thinning behaviour of WPM + D at low $\dot{\gamma}$ values was attenuated. However, unlike with mixtures of D + W[5], the apparent levelling off at high $\dot{\gamma}$ values is delayed to higher $\dot{\gamma}$, i.e., the shear thinning was more uniform across the whole $\dot{\gamma}$ region. This behaviour probably results from the tendency of the WPM particles to entangle and retain their flocculated state until higher shear rates (Sarkar, 2017). The shear thinning of the WPM + D mixture thus represents a hybrid of the behaviour of the individual components.

In order to assess, in more detail, the influence of WPM on $\eta$ of mixtures of WPM + D, in Figure 2 we plot the relative viscosity ($\eta_r = \frac{\eta_s}{\eta_D}$) of the mixtures as a function of Péclet number (*Pe*), defined in equation (4):

$$Pe = \frac{6\pi\dot{\gamma}\eta_D d_H^3}{8k_B T} \tag{4}$$

where, $\eta_s$ and $\eta_D$ are the viscosities of a WPM + D mixture and the corresponding D solution, respectively, whilst $d_H$, $k_B$ and *T* are the hydrodynamic diameter of the WPM particles, Boltzmann constant and temperature, respectively. Figure 2 more clearly illustrates the influence of WPM on $\eta$ of the WPM + D mixtures, *i.e.*, $\eta_r$ > 1 across all mixtures and *Pe* number. WPM and WPM + D[1] showed an identical shear-thinning behaviour and showed a tendency to plateau at *Pe* ≈ 1, indicating similar characteristic times for flow and Brownian diffusion processes (Andablo-Reyes, 2019).

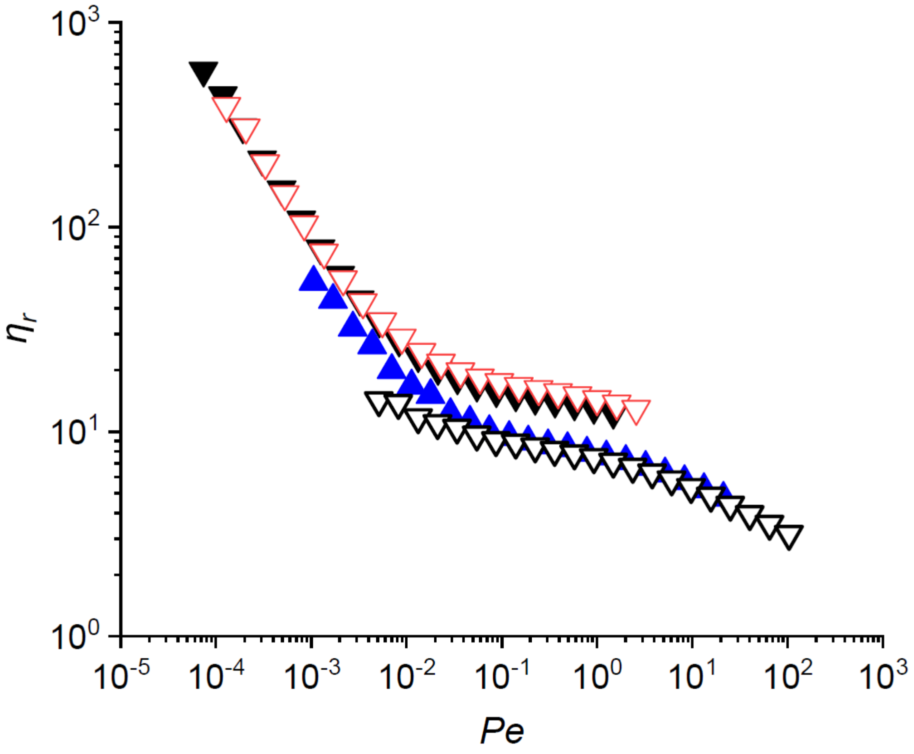

**Figure 2.** Relative shear viscosity of mixtures of microgel and dextran solutions WPM (▼), WPM + D[1] (▽), WPM + D[5] (▲) and WPM + D[11] (▽) as a function of Péclet number (*Pe*).

At *Pe* < 0.01, where diffusive transport should dominate, $\eta_r$ showed a similar behaviour for WPM + D[5] and WPM +D[1] (or WPM alone). At *Pe* > 0.1 the behaviour of WPM + D[5] and WPM + D[11] were identical, up to *Pe* as high as $10^2$. Thus at low $\dot{\gamma}$ and [D] values the interactions between the WPM particles dominate the $\eta$, but at higher $\dot{\gamma}$ and [D] values the $\eta$ is increasingly dominated by the background $\eta$ of the D solutions. Higher [D] presumably helps to disturb the diffusive and flow behaviour of WPM particles resulting in lower $\eta_r$ values at low $\dot{\gamma}$ (disrupted interactions) and delayed Newtonian plateaus at high $\dot{\gamma}$ respectively.

## 3.3. Soft tribology

### *3.3.1 Frictional behaviour of biopolymers, microgels and conjugated systems*

The $\mu$ results obtained using the MTM2 for biopolymer solutions of D and W, mixtures of D and W[5], WPM, mixtures of WPM and D and conjugated systems are shown in Figures 3A and 3B.

***Biopolymers.*** In agreement with the previous findings (Kew, Holmes, Stieger, & Sarkar, 2021; Zembyla, 2021), W[5] decreased the boundary $\mu$ from just over 1 (buffer) to 0.3 (Figure 3A and Figure S3), which suggests adsorption-induced lubricity at the interface, as schematically shown in Figure 4. Theoretically, the boundary regime specifies the complete exclusion of a continuous lubricant film from the contact interface, although local regions of trapped lubricant can exist between soft tribocontacts (Dowson, 1995). The boundary regime is usually taken as the (low) $u$ range at which the $\mu$ becomes relatively independent of $u$, with some variations induced by the lubricant/ material viscoelasticity (Sarkar, 2021; Selway, 2017). The lubrication regimes are often determined qualitatively from the $\mu - u$ graphs.

In general, there is no concrete consensus on the interplay between the extent of surface adsorption and the boundary lubrication behaviour (Sarkar, 2021; Stokes, 2011). However, deposition of soft biopolymers at the interface can alleviate direct surface interactions between contact bodies (asperity-asperity contact) in the boundary regime or via reducing hydrophobic interactions in self-mated PDMS contacts (Lee, Iten, Müller, & Spencer, 2004), hence reducing the boundary $\mu$.

D[1] and D[5] showed a similar boundary $\mu$ to that of the buffer (Figure 3A and Figure S3A), which is in line with previous findings for steel-on-glass (Perrino, 2009) and PDMS-on-steel tribocontacts (Käsdorf, et al., 2017). The lack of propensity of dextran to prompt hydrophobic and/or electrostatic interactions with PDMS surfaces

(Käsdorf, 2017; Perrino, 2009) led to an unfavourably high boundary $\mu$. Note that D[11] has not reach the boundary regime in the MTM2 measurements.

Upon increase of [D], the onset of the elasto-hydrodynamic lubrication (EHL) regime (*i.e.* full-separation of contact-bodies by a thin fluid film at the interface) shifted to lower $u$ values (Figure 3A). This shift is a result of the increased $\eta$ values of the dispersions, as shown in Figure 1A. The minimum $u$ at which the EHL regime was established ($u_{EHL}$), which is associated with the speed at which the minimum friction coefficient ($\mu_{min}$) is often observed, decreased by over an order of magnitude, from ~1 to 0.1 m $s^{-1}$, when the [D] was increased from 1 to 11 wt%. The shift was significant enough to impede the boundary regime at the lowest $u$ measurable (1 mm $s^{-1}$) via the MTM2. This emphasizes the viscous lubricity of D, especially at [D] = 5 and 11 wt%. This is schematically shown in Figure 4, where viscous-driven hydrodynamic forces generate a lifting force *($F_v$ in Figure 4)* which enhances the gap between contacting surfaces. The viscous lubricity of D can also be appreciated in Figure S3A (Supporting Information), where the $\mu$ curves for D[1], D[5] and D[11] collapsed onto a single curve.

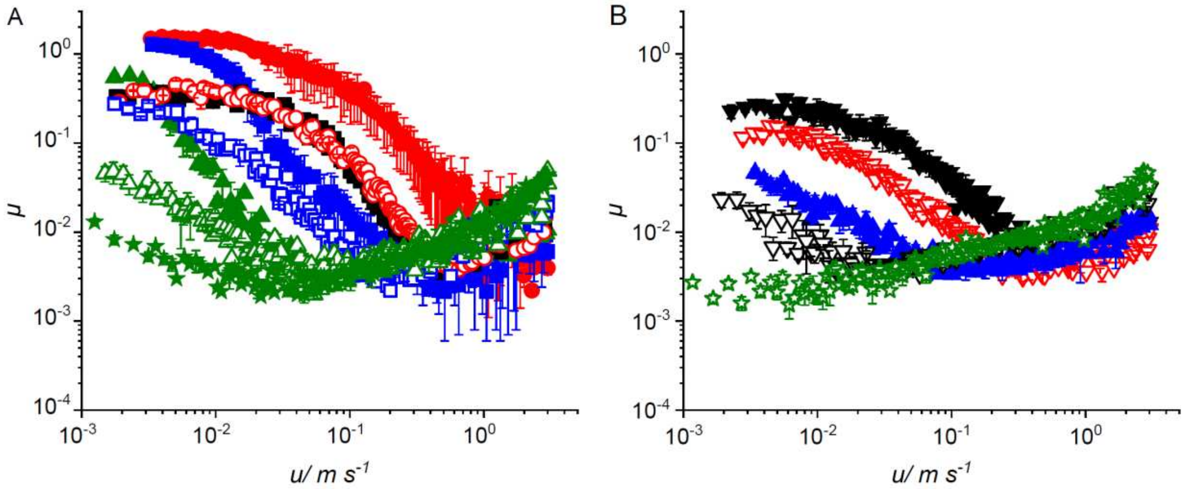

**Figure 3.** (A) Friction coefficient ($\mu$) *versus* entrainment speed ($u$) for biopolymer solutions D[1] (●), D[5] (■), D[11] (▲) and W[5] (■); mixtures of dextran and whey protein D[1] + W[5] (○), D[5] + W[5] (□), D[11] + W[5] (△) and also the conjugate Conj(D[11] + W[5]) (★). (B) $\mu$ *versus* $u$ for the microgel systems WPM (▼), WPM + D[1] (▽), WPM + D[5] (▲), WPM + D[11] (▽), and also conjugated microgel Conj(D[11] + W[5])MG (☆). Means are calculated based on readings on at least triplicate samples (n ≥ 3).

***Biopolymer mixtures.*** The addition of D[1] and D[5] to W[5] gave marked changes to the boundary $\mu$ of W[5] (Figure 3A). This is further evidenced in Figure S3A (Supporting Information) which show the $\mu - \eta_{2000}u$ plots. It is known that hydrophilic neutral coatings can possess anti-fouling properties against protein adsorption (Österberg, et al., 1995). Dextran is part of that category and the anti-fouling characteristics of dextran-coated surfaces (Griesser, et al., 2002; Perrino, 2008) or modified-dextran layered surfaces (Martwiset, Koh, & Chen, 2006; McLean, et al., 2000; Piehler, Brecht, Hehl, & Gauglitz, 1999) are well-documented. Therefore, the same boundary $\mu$ observed for W[5], D[1] + W[5] or D[5] + W[5] indicates the limited adsorption behaviour of D on PDMS, and addition of D to W does not influence the surface-driven lubrication performance of the latter. This suggests that frictional forces in direct surface contacts for D[1] + W[5] and D[5] + W[5] were mainly governed by W adsorbing to the PDMS surfaces.

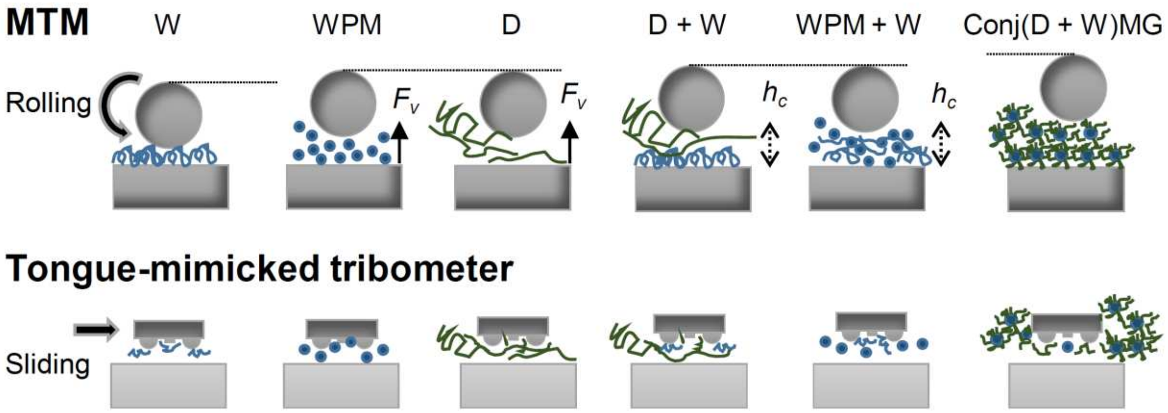

Figure 4. Schematic illustration of governing lubrication mechanisms of the studied dispersions in MTM and 3D tongue-mimicked tribocontacts. Adsorption and probable aggregation of W provided thin-film and hydration lubricity. $F_v$ is the lifting force generated by hydrodynamic/ viscous forces (lubricant viscosity) when D or WPM was added to the system. The central film thickness values ($h_c$) for each pair of systems: D[5] + W[1] and WPM + W[1], D[5] + W[5] and WPM + W[3], and D[5] + W[11] and WPM + W[8], were almost identical as a result of the similar thickening behaviour of WPM and D[5]. The entrainment of Conj(D[11] + W[5])MG particles into the contact interface facilitated cushioning and brush lubrication mechanisms in the MTM measurements, a factor that was lacking in the tongue-mimicked tribocontacts.

Comparing the solutions of D to its mixtures with W[5], it can be seen that W[5] does not influence $u_{EHL}$ of the mixtures considerably (Figure 3A), particularly when the [D] was greater than [W], showing W's trivial viscous-lubricity behaviour. The addition of W[5] to D solutions contributed to the lubrication performance of the mixtures in the mixed regime (clearly reflected in Figure S3A, Supporting Information), where the $\mu$ increases monotonically with decreasing $u$ until it reaches a plateau (*i.e.* the boundary regime). This can be attributed to W adsorption and its contribution to the slight increase in $\eta$ of the dispersions (Figure 1A), though the former is expected to be the dominant factor. In the mixed lubrication regime, the contact surfaces are in close proximity, leading to direct contact of surface asperities whilst a part of the contact load is still borne by the confined fluid (Sarkar, 2021). Therefore, adsorbed layers can still play a role in the mixed regime (Sarkar, 2021) either by lowering the extent of asperity-asperity contacts (Stokes, 2011) and/or by facilitating hydration lubrication (Hu, Andablo-Reyes, Soltanahmadi, & Sarkar, 2020; Klein, 2013; Xu, et al., 2020) via an easy-slip layer (Figure 4).

***Conjugate.*** Interestingly, the conjugate (Conj(D[11] + W[5])) showed a lower mixed $\mu$ as compared to D[11] + W[5] (Figure 3A), despite their almost identical $\eta_{2000}$ (Figure 1A). When D and W (or WPM) are mixed without heat treatment - except for hydrogen bonding - electrostatic interactions, complex formation and conjugation are not expected due to the neutral nature of D (Sun, Yu, Yang, , 2011). However, glycosylation of protein molecules is known to bring about a loss of secondary structure and to mitigate heat-induced aggregation (Sun, Yu, Yang, , 2011).

Flash-heating is a well-known phenomenon in the tribology of solid surfaces and refers to local heating of the contact interface in the event of asperity-asperity contacts under high shear (the mixed and boundary regime). The local heating can be significantly higher than the temperature of the bulk lubricant (Vakis, et al., 2018), with important implications for friction (*e.g.* can lead to phase transformation of hard metals). The literature in relation to flash-heating in oral soft tribology is scarce, probably due to the low temperatures assumed (often 37 °C, emulating physiological conditions) and complexities around viscoelastic energy dissipation (Persson, 2006). The surface roughness, contact geometry and viscoelastic properties influence the lubricant squeeze-out dynamics and hence the $\mu$ (Lorenz, et al., 2013). With flash-heating altering local viscoelastic (asperity level) properties of an elastomer, the squeeze-out dynamics are expected to significantly differ when the elastomer encounters flash-heating. Although the impact of flash-heating on structural change of the surface adsorbed films is usually overlooked, similar concepts on lubricant film collapse have been raised and referred to as ‘de-wetting’ at the asperity level (Selway, 2017). PDMS has a thermal conductivity of around 0.16 W mK$^{-1}$, at least two orders of magnitude lower than that of the bearing steel (AISI 52100) (Reddyhoff, Schmidt, & Spikes, 2019), and thus could undergo a local heating much more easily and within a relatively short period of time when the sliding speed is high enough to make the thermal diffusion negligible (reported to be sliding speed > 0.01 m s$^{-1}$ for *the* rubber (Persson, 2006)).

Considering all the above, we propose that in the event of flash-heating, W-D conjugate molecules will resist aggregation, bringing about a slower rate of de-wetting. Our hypothesis is that, the loss of secondary structure and reduced heat-induced aggregation of Conj(D[11] + W[5]) (Sun, Yu, Yang, , 2011), results in a stacked arrangement of such molecules, aligned parallel to the fluid flow. This will generate a slip plane in which the relative motions of biopolymer chains can dissipate the interfacial frictional stresses. Consequently, the conjugated system (Conj(D[11] + W[5])) shows a considerably lower $\mu$ (at $u < 3 \times 10^{-2}\, m\, s^{-1}$) compared to D[11] + W[5] (Figure 3A). The susceptibility to aggregation of W in the non-conjugated systems (*i.e.* D mixtures with W[5]) in the event of flash-heating may hinder the formation of the proposed stacked arrangement and/or lead to faster fluid squeeze-out as compared to Conj(D[11] + W[5]).

***Microgel systems.*** Figure 3B presents the $\mu$ results for WPM and its dispersion in dextran solutions (WPM + D[1], WPM + D[5], WPM + [11]), and Conj(D[11] + W[5])MG system. In order to achieve a valid comparison, the WPG for all dispersions (except for the Conj(D[11] + W[5])MG) was always prepared from W alone, since D is shown to influence the gelation behaviour of W (Araiza-Calahorra, 2020; Sun, Yu, Yang, , 2011; Sun, Yu, Zeng, , 2011). The lubrication behaviour of whey protein microgels has been previously assessed via the MTM2 to show its influence on $\mu$ across the mixed and boundary lubrication regimes (Andablo-Reyes, 2019; Sarkar, 2017).

In this work, WPM performed similarly to W[5] in the boundary regime (Figure 3B) implying that the adsorbed/trapped layers of whey protein microgel and non-denatured whey protein molecules provided very similar interfacial effects (Figure 4). Interestingly, the $u_{EHL}$ for WPM and W[5] occurred at a similar value (~ 0.4 m s$^{-1}$) despite the fact that the $\eta_{2000}$ of the WPM was over three times larger than that of W[5] (Figure 1). To investigate this observation further, the lubricant film thicknesses and the $\dot{\gamma}$ values at the contact interface in the EHL regime were estimated as follows. The central film thickness ($h_c$) of the microgel-containing dispersions was calculated using the modified Hamrock-Dowson empirical expression (Hamrock & Dowson, 1978; Myant, Fowell, Spikes, & Stokes, 2010):

$$h_c = 3.3R'U^{0.63}W^{-0.13} \tag{5}$$

where, $U$ is the dimensionless speed parameter ($\frac{u\eta_{eff}}{R'E'}$) and W is the dimensionless load parameter ($\frac{F}{E'R'^2}$). The terms $\eta_{eff}$ and $F$ are the effective $\eta$ of the fluid at the extant shear rates relevant to tribological contact (often taken as the second Newtonian plateau in rheological measurements (de Vicente, 2005), $\eta_{2000}$ in this study) and the applied normal load. $R'$ and $E'$ are the effective radius of curvature in the direction of the fluid entrainment and the equivalent modulus of elasticity of PDMS specimens, respectively (Sarkar, 2021). $R'$ and $E'$are given by $\frac{1}{R'} = \frac{1}{R_1} + \frac{1}{R_2}$ and $E' = \frac{2E_1E_2}{E_1(1-\nu_2^2)+E_2(1-\nu_1^2)}$ where, ($E_1$ and $E_2$), ($\nu_1$ and $\nu_2$) and ($R_1$ and $R_2$) are the elastic moduli, Poisson's ratios and the radii of curvature of the two contact bodies 1 and 2 (*i.e.*, the ball and disc), respectively (Sarkar, 2021). Assuming laminar flow with no wall slip, a rough estimation of the $\dot{\gamma}$ can be obtained from $\dot{\gamma} = \frac{SRR.u}{h_c}$. The approximate $\dot{\gamma}$ values together with $u_{EHL}$ and $h_c$ for microgel-containing dispersions are shown in Table 3. The $\dot{\gamma}$ values agree with the values of over $10^3$ claimed for tribological contacts (Stokes, 2013).

**Table 3.** Viscosities of the dispersions at $\dot{\gamma} = 2000$ s$^{-1}$ ($\eta_{2000}$), the entrainment speeds ($u_{EHL}$), the calculated central film thicknesses at the contact interface ($h_c$) and estimated shear rates (Est. $\dot{\gamma}$) in the EHL regime.

| **Dispersions** | **$\eta_{2000}$ (mPa s)** | **$u_{EHL}$ (m s$^{-1}$)** | **$h_c$ (µm)** | **Est. $\dot{\gamma}$ (s$^{-1}$×10$^3$)** |
|---|---|---|---|---|
| WPM | 11 | 0.380 | 3.071 | 61.872 |
| WPM + D[1] | 16 | 0.250 | 2.963 | 42.192 |
| WPM + D[5] | 47 | 0.125 | 3.791 | 16.486 |
| WPM + D[11] | 121 | 0.035 | 3.079 | 5.682 |

| | | | | |
|---|---|---|---|---|
| Conj(D[11] + W[5])MG | 124 | 0.001* | 0.334 | 1.494 |
| WPM + W[1] | 12 | 0.376 | 3.327 | 56.512 |
| WPM + W[3] | 12 | 0.364 | 3.180 | 57.233 |
| WPM + W[8] | 20 | 0.190 | 2.872 | 33.081 |

* The EHL regime could not be accurately identified and a value of 0.001 was assumed as the $u_{EHL}$.

The estimated $\dot{\gamma}$ and $h_c$ for WPM are 30x higher in magnitude than the highest $\dot{\gamma}$ measured with the rheometer (Figure 1) and the WPM particle size (Table 2). This suggests that at a large $h_c/d_h$ and relatively high $\dot{\gamma}$, WPM and W[5] can show similar EHL behaviour. In other words, the impact of particles on the hydrodynamic forces are not significant and WPM can show lower $\eta$ values under extreme $\dot{\gamma}$ values taking place in tribological conditions (*i.e.* $\eta_{2000} \neq \eta_{eff}$ ) which may prompt shear-induced deformation or de-swelling (water loss). This can be attributed to the extreme shear thinning behaviour of non-Newtonian fluids when subjected to high shear rates at the inlet of tribocontacts (Cassin, Heinrich, & Spikes, 2001).

The transition from the boundary regime to the mixed regime occurred at a lower $u$ for WPM compared to that for W[5]. Further, the $\mu$ at $0.01 < u < 0.04$ m s$^{-1}$ was lower for the same comparison (Figure 3B). Using equation (5), the calculated $h_c$ and $h_{min}$(*i.e.* the minimum film thickness, $h_{min} = 2.8R'U^{0.68}W^{-0.20}$) at the above speed range were 0.31 to 0.74 and 0.14 to 0.36 μm, respectively. In the boundary and transition to mixed regimes, $h_{min}$ tends to better represent the actual lubricant film thickness due to a high proportion of asperity-asperity contacts in these regimes. Interestingly, the fall in $\mu$ for WPM took effect at a $u$ value with a corresponding $h_{min}$ value (0.14 μm) just greater than $d_H$ of the WPM (~0.12 μm) and the decrease continued until $h_{min} {\sim} 3 \times d_H$ (0.36 μm). This seems to corroborate the rolling mechanism of WPM (*i.e.* ball bearing) which leads to a $\mu$ reduction when the gap size is equal or slightly larger than the particle size (Sarkar, 2017; Yakubov, Branfield, Bongaerts, & Stokes, 2015). It is also worth noting that rupture of the WPM particles is not expected under the contact pressure used in this study (Andablo-Reyes, 2019). Thus, the structural integrity of the microgels facilitates their entrainment and reduction of the $\mu$ at $u$ values up to at least 0.04 m s$^{-1}$.

For WPM and its dispersions in dextran solutions (Figure 3B) $h_c$ in the EHL regime (2.9 to 3.8 μm) also exceeds the particle sizes (0.124 - 0.135 μm) by at least an order of magnitude (Tables 1 and 3). Thus the large $h_c/d_h$ ratios, together with high $\dot{\gamma}$ values (5 - 42 × 10$^3$ s$^{-1}$) at the contact interfaces (breaking up any particle aggregates) likewise brought about free entrainment of particles into the contact region. The high $\eta$ values of WPM + D[5] and + WPM + D[11] (Figure 1B) shifted $u_{EHL}$ to 0.1-0.3 × $u_{EHL}$ of WPM, impeding tribo-contacts into the boundary regime at the lowest $u$ measurable with the MTM2 (Figure 3B and Figure S3B in Supporting Information).

The $\mu$ of WPM + D[1] in the boundary (and mixed) regime was slightly lower when compared to WPM (Figure 3B), which can be attributed to its higher $\eta$ (Figure 1B) resulting in the lubricant film squeezing out more slowly (Selway, 2017). In soft tribo-contacts, the viscoelasticity of elastomers at asperity scale can further reduce the squeeze out dynamics, as discussed by Dowson two decades ago (Dowson, 1995), referred to as '*micro-EHL*'. Here, deformation of the surface asperities results in perturbation to the local pressure profile that can lead to a persisting lubricant film between surfaces even into the boundary regime (Dowson, 1995). The lower $\mu$ with the addition of D[1] to WPM was not observed for D[1] + W[5] (Figure 3A, also see Figure S3B showing the $\mu - \eta_{2000} \times u$ plots). Our reasoning for this is that, adsorption of W, under these conditions, would probably alter the contact surface properties (wettability, roughness, chemistry and adhesiveness, etc.). This restrains or masks the influence of viscosity on squeeze-out and de-wetting dynamics. As far as we are aware this observation has not been addressed in the literature. Another reason might be that the particulate nature of WPM microgels facilitates separation of contact bodies (not forgetting that they are larger in size compared to the typical surface roughness) and therefore helps to accommodate D chains between the particles and the surfaces.

***Conjugate microgels.*** Conj(D[11] + W[5])MG surpassed all other dispersions in lubricity showing *superlubricity* (*i.e.* resistive forces nearly vanish with friction coefficients < 0.01 within severe tribo-conditions). In the presence of Conj(D[11] + W[5])MG, $\mu$ was around 0.002 at $u\sim 0.001$ m s$^{-1}$ , which significantly exceeded that of WPM + D[11] despite their almost identical viscosities at $\dot{\gamma}$ > 100 s$^{-1}$ (Figures 3B and 1B). Clearly the conjugate microgel particles must have some sort of different structure (*e.g.* altered state of protein unfolding following conjugation (Sun, Yu, Yang, , 2011)) that can influence their adsorption and/or entrainment.

The Conj(D[11] + W[5])MG particles were larger than the WPM but still slightly smaller ($d_H$ = 0.227 μm - see Table 2) than the $h_c$ at 0.001 m s$^{-1}$ (0.334 μm - as shown in Table 3). Considering the low $\dot{\gamma}$ occurring at 0.001 m s$^{-1}$ (estimated as 1494 s$^{-1}$ - see Table 3), particle aggregation is more likely to persist. Therefore, we hypothesize that there is a more aggregated state of these microgel particles (or condensed close-packed state) at $0.001 < u < 0.01$ m s$^{-1}$ which facilitates full separation of contact bodies, alleviating the shear stress at low $u$ via a '*cushioning*' effect, as reflected in Figure 4. The surface interactions in compliant tribo-contacts of PDMS-PDMS involve substantial cohesive and interfacial adhesive friction (Sills, Vorvolakos, Chaudhury, & Overney, 2007) and the cushioning effect by the Conj(D[11] + W[5])MG particles will significantly moderate these resistive forces by hindering hydrophobic-hydrophobic interaction in PDMS-PDMS contacts. A similar mechanism was proposed by Sarkar et al. (Sarkar, 2017) on observation of packed WPM particles at extremely high particle fractions, bringing about $\mu$ values as low as 0.1 on hydrophobic surfaces. The *superlubricity* for Conj(D[11] + W[5])MG could also be attributed to the effect of D chains sticking out the microgels. This will facilitate '*brush-like*' lubrication. Surface adsorbed and grafted dextran (co)polymer chains have shown promising lubrication properties (Goren, 2014; Perrino, 2009; Rosenberg, 2011) depending on the polymer chain conformation and environmental parameters (e.g., pH and solvation). These various possible explanations are schematically illustrated in Figure 4 and need further testing, but it is interesting that the superlubricity of Conj(D[11] + W[5])MG observed in the MTM2 was not observed in the experiments with 3D tongue-mimicked surfaces, discussed later.

### *3.3.2 Comparison of frictional and flow behaviour of combined D[5] + W and WPM + W systems*

The promising viscous and boundary lubricity of WPM suggested that it might be able to deliver similar viscous lubricity as non-conjugated D. It was also noted that D[5] and 41.7 vol% WPM had almost identical $\eta_{2000}$ (9.9 ± 0.4 and 11.0 ± 0.7 mPa s, respectively). Therefore, we performed experiments to examine the flow (Figure 5A) and $\mu$ behaviour (Figure 5B) of W mixtures with D[5] or [WPM] = 41.7 vol%, whilst varying the [W] in free water between 1 and 13 wt% (see Table S1) to moderate the surface interactions.

All mixtures showed shear thinning behaviour, as seen in Figure 5A. Not surprisingly, the shear thinning behaviour of WPM-containing systems was greater than that of the equivalent dispersions with D[5], due to the more shear thinning nature of WPM alone. A second plateau at the $\dot{\gamma} = 2000$ s$^{-1}$ was observed for almost all the mixtures, with only WPM + W[8] showing a statistical deviation of over 5% between the last two consecutive data points (Figure 5A). The inset of Figure 5A shows the measurements between $\dot{\gamma}$ = 500 and 2000 s$^{-1}$ for mixtures of W with D[5] or WPM. Within this range of $\dot{\gamma}$ and at a constant [W] (in free water), the shear thinning behaviour of the mixtures was similar, giving rise to almost the same $\eta_{2000}$ for each of the pairs D[5] + W[1] and WPM + W[1]; D[5] + W[5] and WPM + W[3]; D[5] + W[11] and WPM + W[8] (Figure 5A). Thus the viscous lubrication behaviour for each of the above mentioned pairs in the EHL or hydrodynamic lubrication (*HL*) regimes was expected to be similar (see Figure 4).

At $u \sim 0.001$ m s$^{-1}$, the $\mu$ of D[5] + W[11] and WPM + W[8] did not level off and therefore, the boundary $\mu$ cannot be derived from the MTM2 measurements (Figure 5B). The $\mu$ of D[5] + W[5] at the lowest $u$ approached to that of W[5] (Figures 3A and 4B). For D[5] + W[1] and WPM + W[1], the onset of the boundary regime can be discerned, signalling a lower boundary $\mu$ for WPM + W[1] (Figure 5B) which originates from the greater proportion of surface active moieties when both W and WPM are present and also the potential interposition of W between the microgel particles (Figure 4). The $\mu$ curve for D[5] + W[1] (Figure 5B) suggested that the boundary $\mu$ would eventually settle at values higher than for W[5], anticipated by the concentration-dependant friction reduction behaviour of W observed elsewhere (Zembyla, 2021).

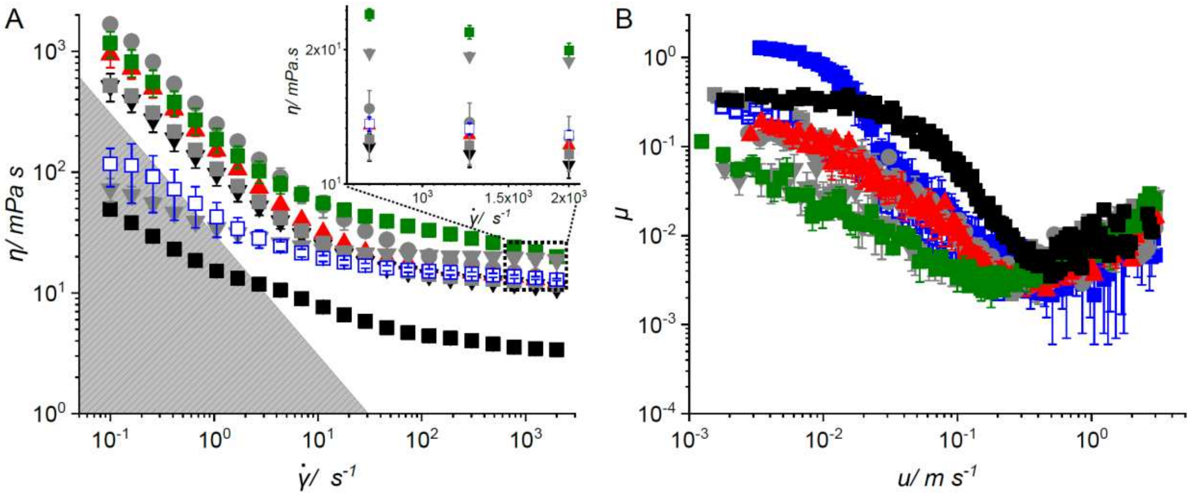

**Figure 5.** Comparison of (A) flow curves and (B) friction coefficient results for: microgel + whey protein mixtures WPM + W[1] (●), WPM + W[3] (▲), WPM + W[8] (🟩) against dextran + whey protein mixtures D[5] + W[1] (■), D[5] + W[5] (□), and D[5] + W[11] (▼). The inset in A shows a zoomed in view for shear rates between 500 and 2000 $s^{-1}$. Note the whey protein concentration in free water (i.e., water content excluding WPM or D) was the same for each of the pairs D[5] + W[1] and WPM + W[1]; D[5] + W[5] and WPM + W[3]; D[5] + W[11] and WPM + W[8]. (For more information see Table S1).

An interesting finding was observed in the mixed lubrication regime where the $\mu - u$ curves overlapped for each of the afore-mentioned pairs (Figure 5B). This observation has two important implications, which are as follows:

(i) The colloidal dispersions of WPM particles behave as a Newtonian fluid within the tribologically-relevant $\dot{\gamma}$ values in the mixed regime and conditions defined in this work. Using eq. (5), $h_c$ values were calculated for WPM dispersion in W solutions at $u$ values reflecting the mixed regime just before its transition to the boundary regime. These values were set at 0.015 and 0.01 m s$^{-1}$ for WPM + W[1] and

WPM + W[3], respectively. A value of 0.002 m $s^{-1}$ was assumed for WPM + W[8], since the transition to the boundary was not evident (Figure 5B). The corresponding $h_c$ values were 0.437, 0.330 and 0.163 µm in order of increasing [W], which are 1.5 - 3.8× higher than the size of the WPM. Thus at $h_c/d_h > \sim 2$ and these correspondingly high shear rates ($\dot{\gamma}$ > $10^4$ $s^{-1}$) the WPM dispersions showed Newtonian behaviour in the mixed regime. A more detailed study is required to assess the critical $h_c/d_h$ ratio, the rheological parameters and microgel properties at which the microgel particles behave in Newtonian manner, particularly when the hydrodynamic forces are not sufficient to fully separate contact bodies.

(ii) By optimising a combination of WPM and (non-microgelled) W, combined viscous and thin-film lubricity could be achieved through a single-component, i.e., whey protein, without the need of any polysaccharide. In this way, proteinaceous lubricants could be developed with no need for including a lipid or polysaccharide component but still meeting the satiety requirements.

In order to further elucidate the mechanism of action of WPM in its mixtures with W, we plotted the $\mu$ curves in Figure 5B as a function of reduced speed parameter, $\eta_{2000} \times u$, (de Vicente, 2005; Sarkar, 2021) as shown in Figure 6. For Newtonian fluids with no apparent surface interactions (*e.g.* adsorption or bonding) or viscous-driven surface separation effects, the shear stresses at the contact surfaces are expected to be independent of the lubricant $\eta$ and the $\mu - \eta_{2000} \times u$ curves are expected to collapse into a single '*master*' curve, shown as the solid grey line in Figure 6.

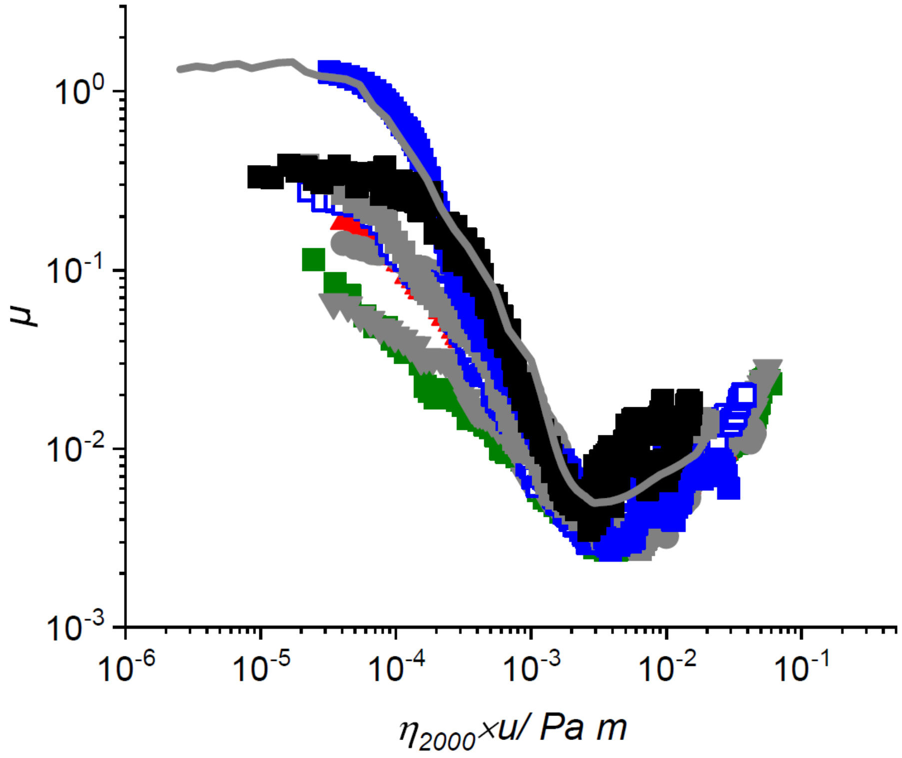

**Figure 6.** Friction curves normalised to the viscosity at a shear rate of 2000 $s^{-1}$ for microgel and whey protein mixtures WPM + W[1] (●), WPM + W[3] (▲), WPM + W[8] (🟩) and also for dextran + whey protein mixtures D[5] + W[1] (■), D[5] + W[5] (□), and D[5] + W[11] (▼). The solid-grey line is the curve for a Newtonian fluid (see text). For clarity, the error bars are excluded from graphs.

Figure 6 shows a similar *EHL* or *HL* $\mu$ value for each of the compared pairs. Also, $u_{EHL}$ was similar for the Newtonian fluid and mixtures of D + W or WPM + W, in agreement with the observations of Andablo-Reyes, et al. (Andablo-Reyes, 2019). This work demonstrated that the lubrication performance of colloidal WPM dispersions in the *EHL* and *HL* regimes can be approximated as Newtonian fluids (Andablo-Reyes, 2019). This originates from the fact that the predominant source of friction in the *HL* regime is the viscous drag within the lubricant (Andablo-Reyes, 2019; Sarkar, 2021).

Upon addition of WPM or D[5] to W[1] solutions, the absolute value of the characteristic tangent to the $\mu{-}\eta_{2000} \times u$ curve in mixed regime decreased (Figure 6) with an increase in $\eta_{2000}$ (see Figure 5A). Further increase in [W] (*i.e.* WPM + W[3] and D[5] + W[5]) did not show a noticeable influence on the mixed $\mu$ (Figure 6) or on the $\eta_{2000}$ results (Figure 5A). The most distinct decrease in the mixed $\mu$ was observed at the highest [W] (*i.e.* WPM + W[8] and D[5] + W[11]), coinciding with the largest increase in the $\eta_{2000}$. These observations concur with those of Selway et al. (Selway, 2017) and corroborate our findings presented in the previous section: the viscous forces impede fluid squeeze-out and de-wetting of the contacts at the asperity level and therefore reduce the collision frequency between asperities.

### *3.3.3 Soft tribology using tongue-mimicked surfaces*

Due to the lengthy procedures in preparing and cleaning the soft tribology surfaces, not all the above combinations of W, D and WPM were tested with these surfaces. Rather we focussed on those systems that showed the most interesting and unexpected behaviour as evidenced by the MTM2 measurements to provide insights into their lubricity when surface topography, elasticity and wettability emulate the papillae and tribologically relevant features of real human tongue surfaces.

The $\mu$ results for HEPES buffer, W[5], D[11], D[5] + W[5], D[11] + W[5], D[5] + W[11] and also microgel systems (WPM, WPM + D[11] and Conj(D[11] + W[5])MG) are shown in Figure 7A. Fluctuations in the $\mu$ are probably due to the roughness of the deformable elastomer (*i.e.* filiform and fungiform-papillae) and flat-on-flat tribo-testing geometry. Except for solutions with [D] = 11 wt% and the conjugate microgel, the $\mu$ remained almost constant at 0.2 – 0.3 at $5 \times 10^{-5} < u < 10^{-2}$ m s$^{-1}$, 60% lower than for the buffer.

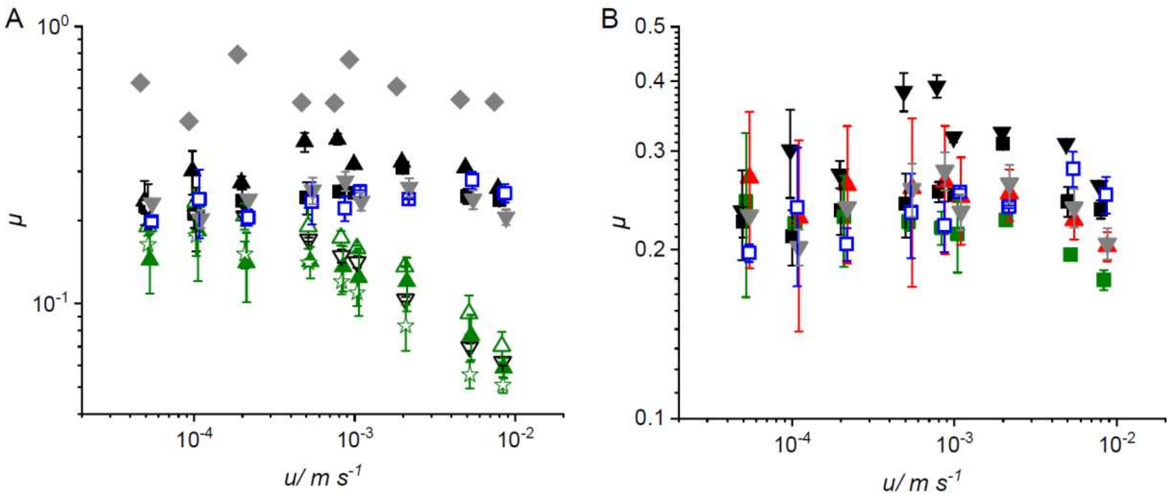

**Figure 7.** (A) Friction coefficient ($\mu$) *versus* entrainment speed ($u$) measured using 3D tongue-mimicking surfaces for: buffer (♦), W[5] (■), D[11] (▲), D[5] + W[5] (□), D[11] + W[5] (△),D[5] + W[11] (▼) and also microgel systems WPM (▼), WPM + D[11] (▽) and Conj(D[11] + W[5])MG (★). (B) Comparison of $\mu$ *versus* $u$ for D[5] + W[5] (□), D[5] + W[11] (▼), WPM + W[3] (▲) and WPM + W[8] (■). Means are calculated based on readings on at least triplicate samples (n ≥ 3). Note the fluctuations in the $\mu$ are probably due to the filiform and fungiform-papillae induced roughness of the deformable elastomer used and flat-on-flat tribo-testing geometry.

The flat-on-flat testing configuration lacks the converging contact wedge at the contact inlet (found in ball-on-disc contacts) which mainly supports the build-up of fluid pressurisation and hydrodynamic lift forces to form a lubricant film (see Figure 4). Therefore, the speed-dependant pressurisation of the fluid trapped between the papillae is not expected to contribute to lubricity except through the '*boosted*' mechanism (Walker, Dowson, Longfield, & Wright, 1968). This is particularly valid considering the high permeability of the fluid through the gaps between papillae (de Boer, et al., 2020). Therefore, the origin of friction in this configuration is a sum of shear stresses experienced by individual papillae, particularly fungiform-mimicked domes, which will be more likely to be in contact with the counter body (*i.e.* the steel plate). The monotonic $\mu$ behaviour of WPM, W[5] and D[5] + W[5] and D[5] + W[11] dispersions (Figure 7A) implies solid-solid contacts between the bodies with the lower $\mu$ values (compared to that of the buffer) indicating a '*thin-film hydration'* mechanism offered by the hydrophilic dispersed phase (*i.e.* WPM, W and D) (Andablo-Reyes, 2020; Klein, 2013; Sarkar, 2021).

The dispersions with [D] = 11% and Conj(D[11] + W[5])MG) showed similar $\mu$ values to other dispersions at $5 \times 10^{-5} < u < 10^{-4}$ m s$^{-1}$, suggesting a boundary regime (Figure 7A). This was followed by a linear drop in $\mu$ values as a function of increasing speed, reaching values between 0.05 and 0.07. The dome-shaped nature of mimicked-fungiform probably provides a converging contact inlet and therefore promotes hydrodynamic forces upon increase in sliding speed, which scale up with increased $\eta$ values. Therefore, at higher speeds (with the high viscosity fluids*,* 0.037 to 0.124 Pa) the fluid was probably forced into the contact zone, bringing about a drop in $\mu$ and transition into the mixed regime.

The other noteworthy observation is the overlapping boundary $\mu$ of D[11] with those of W[5] or WPM-containing dispersions (Figure 7A), in contrast to the MTM2 results (Figures 3A and 3B). This might be attributed to enhanced wettability of the contact surfaces in the tongue-mimicked system decaying dynamic lubricant de-wetting and extending the micro-EHL into the boundary regime (Dowson, 1995), since the squeeze-out dynamics will be hampered by the stronger spread of the lubricant. An additional observation is that Conj(D[11] + W[5])MG) showed no outstanding benefit (Figure 7A), unlike the superlubricous behaviour that this system showed in the MTM2 measurements. This might be due to the absence of: (i) the rolling contact (*i.e.* 3D tongue-mimicking setup operates under pure sliding) which is of paramount importance in entrainment of particles into the contact interface (Yakubov, 2015); or (ii) *cushioning* effect in the tongue-mimic surfaces. Using eq. 5, the calculated $h_c$ and $h_{min}$ at $u = 10^{-4}$ m s$^{-1}$ - the speed just before transition to the mixed regime - were 0.067 and 0.029 µm, respectively. These contact gap dimensions are at least three times smaller than the $d_H$ of the Conj(D[11] + W[5])MG) particles (see Table 2). As shown schematically in Figure 4, this would clearly prevent the cushioning effect and particle entrainment especially in the absence of rolling contacts.

There are notable differences between the tribotests with the MTM2 and the tongue-mimic setup, including their contact configuration and materials. Soft oral tribology examinations using MTM2 have been often performed under combined rolling-sliding contacts which incorporate rolling friction, a factor absent in the 3D-mimicked setup. The contribution of rolling friction in mouth is still ambiguous and needs more attention. In the MTM2, the large compliant contact area (15.2 mm$^2$) compared to that of the tongue-mimicked setup (0.3 mm$^2$), as estimated by Hertzian contact theory, dominates lubricant entrainment and escalates any particle exclusion or confinement effects, whilst the tongue-mimicked setup is a much more realistic representation of tribo-contacts in the mouth, where particle confinement is only likely to occur locally, around papillae features. Furthermore, the large compliant contact area in the MTM2 is likely to accelerate fluid-film squeeze-out (Lorenz, 2013), whilst the textured topography of the tongue mimic (and the tongue) can provide a sustained reservoir of lubricant feeding the contact interface (*i.e. boosted* lubrication) (Walker, 1968). Surface patterning has recently gained significant interest in tribology as a way of providing improved lubricity and load-carrying capacity of lubricant films (Gachot, Rosenkranz, Hsu, & Costa, 2017; He, Chen, & Jane Wang, 2008; Murarash, Itovich,

& Varenberg, 2011). Nature has probably selected the optimized tongue topography to deliver just the right lubricity and perception simultaneously.

In order to verify that WPM provides the same thickening effect as D[5] but also thin-film lubricity, mixtures of WPM or D[5] with W were also investigated on the tongue mimic setup. The results are shown in Figure 7B and it is seen that $\mu$ of all the mixtures remained the same at 0.2 to 0.3 until the $u \sim 5 \times 10^{-3}$ m $s^{-1}$. The higher bulk viscosity mixtures (i.e., D[5] + W[11] and WPM + W[8]) appeared to exhibit a transition between boundary and mixed lubrication regimes manifested in a slight drop in the $\mu$ at $u >$ $5 \times 10^{-3}$ m/s, again due to a slower lubricant squeeze-out. The slightly improved boundary lubricity of mixtures of WPM + W as compared to D[5] + W (MTM2 results, Figure 5B), was not obvious with the tongue-mimicked setup probably due to the aforementioned differences. Apart from this, the results in Figure 7B corroborate the findings with the MTM2 and confirm that proteinaceous microgels can deliver the same desirable effect of polysaccharides. Thus, intelligently combining proteinaceous microgels plus free (non-microgelled) protein may be able to satisfy both the viscous and thin-film lubricity required and food design requirements, whilst aiding clean label designation.

# Conclusions

This study examined the oral-tribological and flow behaviour of Newtonian D solutions when combined with W and their corresponding microgels. PDMS ball on disk friction measurements demonstrated the ability of D and W to provide *viscous* and *thin-film* lubricity, respectively, and the contribution of viscosity-induced enhanced *dynamic-wetting* of surfaces, hence lower friction coefficients, only when they were mixed. W microgels (WPM) imparted *thin-film* lubricity*,* probably through a *rolling* mechanism, and *viscous* lubricity to almost the same extent as obtained with W[5] and D[5], respectively. Combined WPM + D systems showed a similar enhanced *dynamic-wetting* with boosted *viscous lubricity*, due to the enhanced bulk viscosity of these mixtures. Microgels formed from the W-D conjugate, Conj(D[11] + W[5])MG , showed superlubricity behaviour in the ball-on-disk measurements, where the lubricant film thickness was estimated to be of the order of the hydrodynamic size of the microgel particles. We hypothesized that this may be due to a *cushioning lubrication* mechanism where the contact bodies are fully separated by a closely-packed layer of microgels. However, the superlubricity of Conj(D[11] + W[5])MG was not evident in friction measurements with a tongue mimic surface mounted onto the top surface of a cone and plate rheometer type apparatus (against stainless steel as the lower plate). This was attributed to much lower calculated surface contact separations and a lack of rolling contacts in the tongue-mimic setup. Measurements with both types of tribometer showed that combinations of W and WPM should be able to provide desirable oral lubricity and mouth feel without resorting to combinations of polysaccharide additives and fat/oil dispersions. This would bring about a new perspective for food manufacturers in terms of reformulation by minimizing the number of additives used, without compromising any pleasurable mouth-feel.

## Acknowledgement

This study was funded by the European Research Council (ERC) under the European Un-ion's Horizon 2020 research and innovation programme (Grant agreement n° 757993 and 890644) and was carried out at the University of Leeds.

## References

Andablo-Reyes, E., Bryant, M., Neville, A., Hyde, P., Sarkar, R., Francis, M., & Sarkar, A. (2020). 3D biomimetic tongue-emulating surfaces for tribological applications. *ACS Applied Materials & Interfaces, 12*(44), 49371-49385.

Andablo-Reyes, E., Yerani, D., Fu, M., Liamas, E., Connell, S., Torres, O., & Sarkar, A. (2019). Microgels as viscosity modifiers influence lubrication performance of continuum. *Soft Matter, 15*(47), 9614-9624.

Araiza-Calahorra, A., Glover, Z. J., Akhtar, M., & Sarkar, A. (2020). Conjugate microgel-stabilized Pickering emulsions: Role in delaying gastric digestion. *Food Hydrocolloids, 105*, 105794.

Carrasco, F., Chornet, E., Overend, R. P., & Costa, J. (1989). A generalized correlation for the viscosity of dextrans in aqueous solutions as a function of temperature, concentration, and molecular weight at low shear rates. *37*(8), 2087-2098.

Cassin, G., Heinrich, E., & Spikes, H. A. (2001). The influence of surface roughness on the lubrication properties of adsorbing and non-adsorbing biopolymers. *Tribology Letters, 11*(2), 95-102.

de Boer, G. N., Raske, N., Soltanahmadi, S., Dowson, D., Bryant, M. G., & Hewson, R. W. (2020). A porohyperelastic lubrication model for articular cartilage in the natural synovial joint. *Tribology International, 149*, 105760.

de Vicente, J., Stokes, J. R., & Spikes, H. A. (2005). The frictional properties of Newtonian fluids in rolling–sliding soft-EHL contact. *Tribology Letters, 20*(3), 273-286.

Dissanayake, M., Ramchandran, L., & Vasiljevic, T. (2013). Influence of pH and protein concentration on rheological properties of whey protein dispersions. *International Food Research Journal, 20*(5), 2167.

Dowson, D. (1995). Elastohydrodynamic and micro-elastohydrodynamic lubrication. *Wear, 190*(2), 125-138.

Gachot, C., Rosenkranz, A., Hsu, S. M., & Costa, H. L. (2017). A critical assessment of surface texturing for friction and wear improvement. *Wear, 372-373*, 21-41.

Goren, T., Spencer, N., & Crockett, R. J. R. A. (2014). Impact of chain morphology on the lubricity of surface-grafted polysaccharides. *4*(41), 21497-21503.

Griesser, H. J., Hartley, P. G., McArthur, S. L., McLean, K. M., Meagher, L., & Thissen, H. (2002). Interfacial properties and protein resistance of nano-scale polysaccharide coatings. *Smart Materials and Structures, 11*(5), 652-661.

Hamrock, B. J., & Dowson, D. (1978). Elastohydrodynamic lubrication of elliptical contacts for materials of low elastic modulus I—fully flooded conjunction. *Journal of Lubrication Technology, 100*(2), 236-245.

He, B., Chen, W., & Jane Wang, Q. (2008). Surface texture effect on friction of a microtextured poly(dimethylsiloxane) (PDMS). *Tribology Letters, 31*(3), 187.

Hu, J., Andablo-Reyes, E., Soltanahmadi, S., & Sarkar, A. (2020). Synergistic microgel-reinforced hydrogels as high-performance lubricants. *ACS Macro Letters, 9*(12), 1726-1731.

Käsdorf, B. T., Weber, F., Petrou, G., Srivastava, V., Crouzier, T., & Lieleg, O. (2017). Mucin-inspired lubrication on hydrophobic surfaces. *Biomacromolecules, 18*(8), 2454-2462.

Kew, B., Holmes, M., Stieger, M., & Sarkar, A. (2021). Oral tribology, adsorption and rheology of alternative food proteins. *Food Hydrocolloids, 116*, 106636.

Klein, J. (2013). Hydration lubrication. *Friction, 1*(1), 1-23.

Lee, S., Iten, R., Müller, M., & Spencer, N. D. (2004). Influence of molecular architecture on the adsorption of poly(ethylene oxide)−poly(propylene oxide)−poly(ethylene oxide) on PDMS surfaces and implications for aqueous lubrication. *Macromolecules, 37*(22), 8349-8356.

Liu, K., Tian, Y., Stieger, M., van der Linden, E., & van de Velde, F. (2016). Evidence for ball-bearing mechanism of microparticulated whey protein as fat replacer in liquid and semi-solid multi-component model foods. *Food Hydrocolloids, 52*, 403-414.

Lorenz, B., Krick, B. A., Rodriguez, N., Sawyer, W. G., Mangiagalli, P., & Persson, B. N. J. (2013). Static or breakloose friction for lubricated contacts: the role of surface roughness and dewetting. *Journal of Physics: Condensed Matter, 25*(44), 445013.

Martwiset, S., Koh, A. E., & Chen, W. (2006). Nonfouling characteristics of dextran-containing surfaces. *Langmuir, 22*(19), 8192-8196.

McLean, K. M., Johnson, G., Chatelier, R. C., Beumer, G. J., Steele, J. G., & Griesser, H. J. (2000). Method of immobilization of carboxymethyl-dextran affects resistance to tissue and cell colonization. *Colloids and Surfaces B: Biointerfaces, 18*(3), 221-234.

Murarash, B., Itovich, Y., & Varenberg, M. (2011). Tuning elastomer friction by hexagonal surface patterning. *Soft Matter, 7*(12), 5553-5557.

Myant, C., Fowell, M., Spikes, H. A., & Stokes, J. R. (2010). An investigation of lubricant film thickness in sliding compliant contacts. *Tribology Transactions, 53*(5), 684-694.

Oliver, C. M., Melton, L. D., & Stanley, R. A. (2006). Creating proteins with novel functionality via the Maillard reaction: A review. *Critical Reviews in Food Science and Nutrition, 46*(4), 337-350.

Österberg, E., Bergström, K., Holmberg, K., Schuman, T. P., Riggs, J. A., Burns, N. L., Van Alstine, J. M., & Harris, J. M. (1995). Protein-rejecting ability of surface-bound dextran in end-on and side-on configurations: Comparison to PEG. *29*(6), 741-747.

Perrino, C., Lee, S., Choi, S. W., Maruyama, A., & Spencer, N. D. (2008). A biomimetic alternative to poly(ethylene glycol) as an antifouling coating: resistance to nonspecific protein adsorption of poly(l-lysine)-graft-dextran. *Langmuir, 24*(16), 8850-8856.

Perrino, C., Lee, S., & Spencer, N. D. (2009). End-grafted sugar chains as aqueous lubricant additives: synthesis and macrotribological tests of poly(l-lysine)-graft-dextran (PLL-g-dex) copolymers. *Tribology Letters, 33*(2), 83-96.

Persson, B. N. (2006). Rubber friction: role of the flash temperature. *Journal of Physics: Condensed Matter, 18*(32), 7789.

Piehler, J., Brecht, A., Hehl, K., & Gauglitz, G. (1999). Protein interactions in covalently attached dextran layers. *Colloids and Surfaces B: Biointerfaces, 13*(6), 325-336.

Pradal, C., & Stokes, J. R. (2016). Oral tribology: bridging the gap between physical measurements and sensory experience. *Current Opinion in Food Science, 9*, 34-41.

Rao, M. A. (2014). Flow and functional models for rheological properties of fluid foods. In *Rheology of Fluid, Semisolid, and Solid Foods: Principles and Applications* (pp. 27-61). Boston, MA: Springer US.

Reddyhoff, T., Schmidt, A., & Spikes, H. (2019). Thermal conductivity and flash temperature. *Tribology Letters, 67*(1), 22.

Rosenberg, K. J., Goren, T., Crockett, R., & Spencer, N. D. (2011). Load-induced transitions in the lubricity of adsorbed poly(l-lysine)-g-dextran as a function of polysaccharide chain density. *ACS Applied Materials & Interfaces, 3*(8), 3020-3025.

Sarkar, A., Andablo-Reyes, E., Bryant, M., Dowson, D., & Neville, A. (2019). Lubrication of soft oral surfaces. *Current Opinion in Colloid & Interface Science, 39*, 61-75.

Sarkar, A., Kanti, F., Gulotta, A., Murray, B. S., & Zhang, S. (2017). Aqueous lubrication, structure and rheological properties of whey protein microgel particles. *Langmuir, 33*(51), 14699-14708.

Sarkar, A., & Krop, E. M. (2019). Marrying oral tribology to sensory perception: a systematic review. *Current Opinion in Food Science, 27*, 64-73.

Sarkar, A., Murray, B., Holmes, M., Ettelaie, R., Abdalla, A., & Yang, X. (2016). In vitro digestion of Pickering emulsions stabilized by soft whey protein microgel particles: influence of thermal treatment. *Soft Matter, 12*(15), 3558-3569.

Sarkar, A., Soltanahmadi, S., Chen, J., & Stokes, J. R. (2021). Oral tribology: Providing insight into oral processing of food colloids. *Food Hydrocolloids, 117*, 106635.

Selway, N., Chan, V., & Stokes, J. R. (2017). Influence of fluid viscosity and wetting on multiscale viscoelastic lubrication in soft tribological contacts. *Soft Matter, 13*(8), 1702-1715.

Sills, S., Vorvolakos, K., Chaudhury, M. K., & Overney, R. M. (2007). Molecular origins of elastomeric friction. In E. Gnecco & E. Meyer (Eds.), *Fundamentals of Friction and Wear* (pp. 659-676). Berlin, Heidelberg: Springer Berlin Heidelberg.

Stokes, J. R., Boehm, M. W., & Baier, S. K. (2013). Oral processing, texture and mouthfeel: From rheology to tribology and beyond. *Current Opinion in Colloid & Interface Science, 18*(4), 349-359.

Stokes, J. R., Macakova, L., Chojnicka-Paszun, A., de Kruif, C. G., & de Jongh, H. H. J. (2011). Lubrication, adsorption, and rheology of aqueous polysaccharide Solutions. *Langmuir, 27*(7), 3474-3484.

Sun, W.-W., Yu, S.-J., Yang, X.-Q., Wang, J.-M., Zhang, J.-B., Zhang, Y., & Zheng, E.-L. (2011). Study on the rheological properties of heat-induced whey protein isolate–dextran conjugate gel. *Food Research International, 44*(10), 3259-3263.

Sun, W.-W., Yu, S.-J., Zeng, X.-A., Yang, X.-Q., & Jia, X. (2011). Properties of whey protein isolate–dextran conjugate prepared using pulsed electric field. *Food Research International, 44*(4), 1052-1058.

Tirtaatmadja, V., Dunstan, D. E., & Boger, D. V. (2001). Rheology of dextran solutions. *Journal of Non-Newtonian Fluid Mechanics, 97*(2), 295-301.

Vakis, A. I., Yastrebov, V. A., Scheibert, J., Nicola, L., Dini, D., Minfray, C., Almqvist, A., Paggi, M., Lee, S., Limbert, G., Molinari, J. F., Anciaux, G., Aghababaei, R., Echeverri Restrepo, S., Papangelo, A., Cammarata, A., Nicolini, P., Putignano, C., Carbone, G., Stupkiewicz, S., Lengiewicz, J., Costagliola, G., Bosia, F., Guarino, R., Pugno, N. M., Müser, M. H., & Ciavarella, M. (2018). Modeling and simulation in tribology across scales: An overview. *Tribology International, 125*, 169-199.

Walker, P. S., Dowson, D., Longfield, M. D., & Wright, V. (1968). "Boosted lubrication" in synovial joints by fluid entrapment and enrichment. *Annals of the rheumatic diseases, 27*(6), 512-520.

Xu, F., Liamas, E., Bryant, M., Adedeji, A. F., Andablo-Reyes, E., Castronovo, M., Ettelaie, R., Charpentier, T. V. J., & Sarkar, A. (2020). A self-assembled binary protein model explains high-performance salivary lubrication from macro to nanoscale. *Advanced Materials Interfaces, 7*(1), 1901549.

Yakubov, G. E., Branfield, T. E., Bongaerts, J. H. H., & Stokes, J. R. (2015). Tribology of particle suspensions in rolling-sliding soft contacts. *Biotribology, 3*, 1-10.

Yang, X., Li, A., Li, X., Sun, L., & Guo, Y. (2020). An overview of classifications, properties of food polysaccharides and their links to applications in improving food textures. *Trends in Food Science & Technology, 102*, 1-15.

Zembyla, M., Liamas, E., Andablo-Reyes, E., Gu, K., Krop, E. M., Kew, B., & Sarkar, A. (2021). Surface adsorption and lubrication properties of plant and dairy proteins: A comparative study. *Food Hydrocolloids, 111*, 106364.

## CRediT author statement

**Dr. Siavash Soltanahmadi:** Conceptualization, Methodology, Validation, Formal analysis, Investigation, Data curation, Writing- Reviewing & Editing; Visualization; Project administration; Writing- Original draft preparation, Writing- Reviewing & Editing**, Prof. Brent S. Murray:** Conceptualization, Supervision, Writing- Reviewing & Editing; Prof. **Anwesha Sarkar:** Conceptualization, Project administration**;** Writing- Reviewing & Editing, Supervision, Funding acquisition**.**

## Conflict of Interests

Declarations of interest: none

**Supporting information**

# Comparison of oral tribological performance of proteinaceous microgel systems with protein-polysaccharide combinations

Siavash Soltanahmadi, Brent S. Murray, Anwesha Sarkar*

Food Colloids and Bioprocessing Group, School of Food Science and Nutrition,
University of Leeds, UK

*Corresponding author:
Prof. Anwesha Sarkar
Food Colloids and Processing Group,
School of Food Science and Nutrition, University of Leeds, Leeds LS2 9JT, UK.
E-mail address: A.Sarkar@leeds.ac.uk (A. Sarkar).

**Table S1**. The composition of the whey protein mixtures with D[5] or WPM.

| Sample name | Dextran (wt%)* | Whey protein (wt%)* | Whey protein in free water (wt%)‡ | Whey protein microgel (vol%)* |
|---|---|---|---|---|
| D[5]+ W[1] | 5 | 1 | 1.06 | - |
| D[5] + W[5] | 5 | 5 | 5.59 | - |
| D[5] + W[11] | 5 | 11 | 13.27 | - |
| WPM + W[1] | - | 0.62 | 1.06 | 41.7 |
| WPM + W[3] | - | 3.26 | 5.59 | 41.7 |
| WPM + W[8] | - | 7.74 | 13.27 | 41.7 |

* The values show the concentrations of the relevant biopolymers (pristine or conjugated) in the total weight/volume of the dispersions.

‡ The values present the concentration of whey protein in free water content (*i.e.* excluding D or WPM and the water trapped in the cross-linked network of WPM) of the mixtures.

Due to the particulate nature of WPM and therefore, for true companions between the influence of D[5] and WPM on flow and lubrication behaviour of their mixtures with whey protein solutions, the concentration of whey protein in free water (i.e. water content excluding WPM or D) was set to be the same for each comparison-pair of D[5] + W[1] and WPM + W[1]; D[5] + W[5] and WPM + W[3]; and D[5] + W[11] and WPM + W[8]. The comparison classes are shaded with the same colour in Table S1.

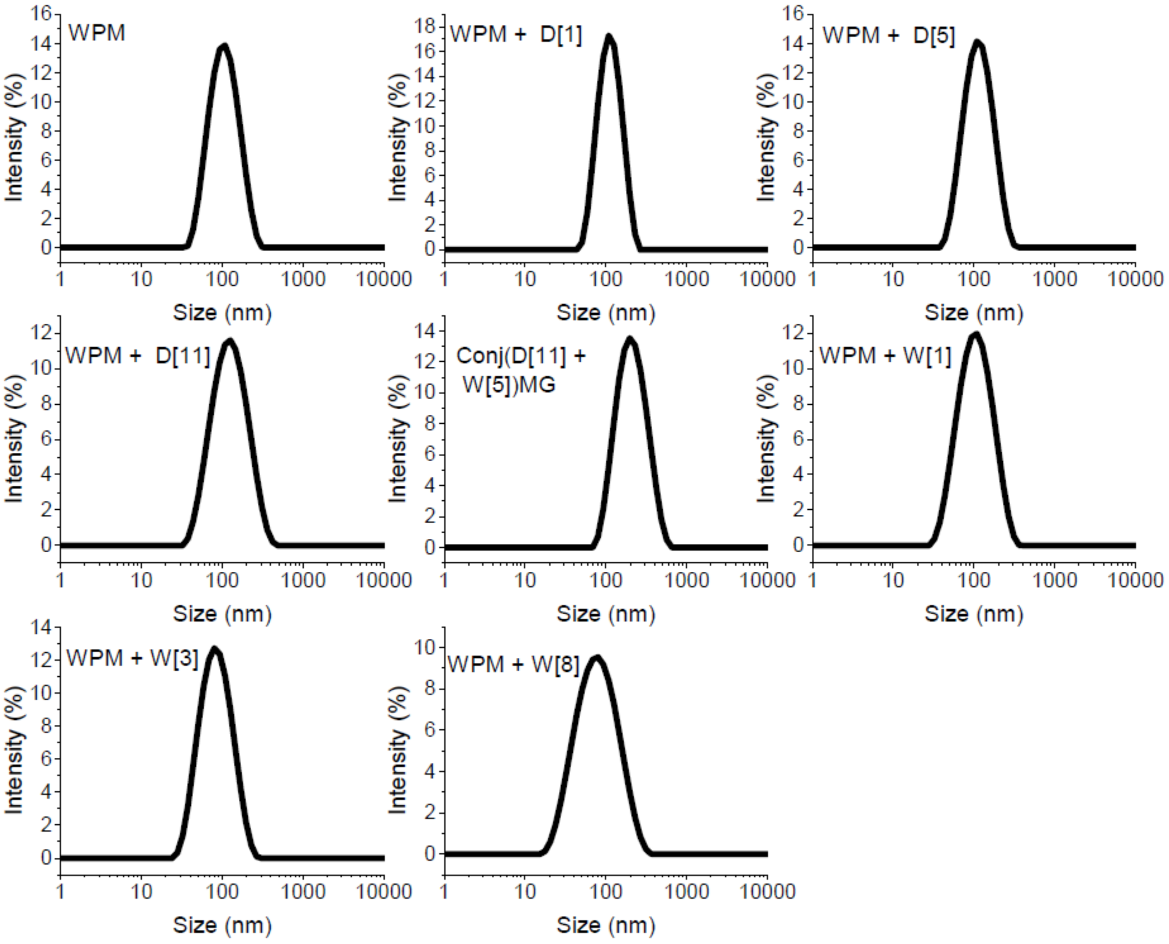

**Figure S1.** Typical results obtained for size measurements using DLS for microgel systems.

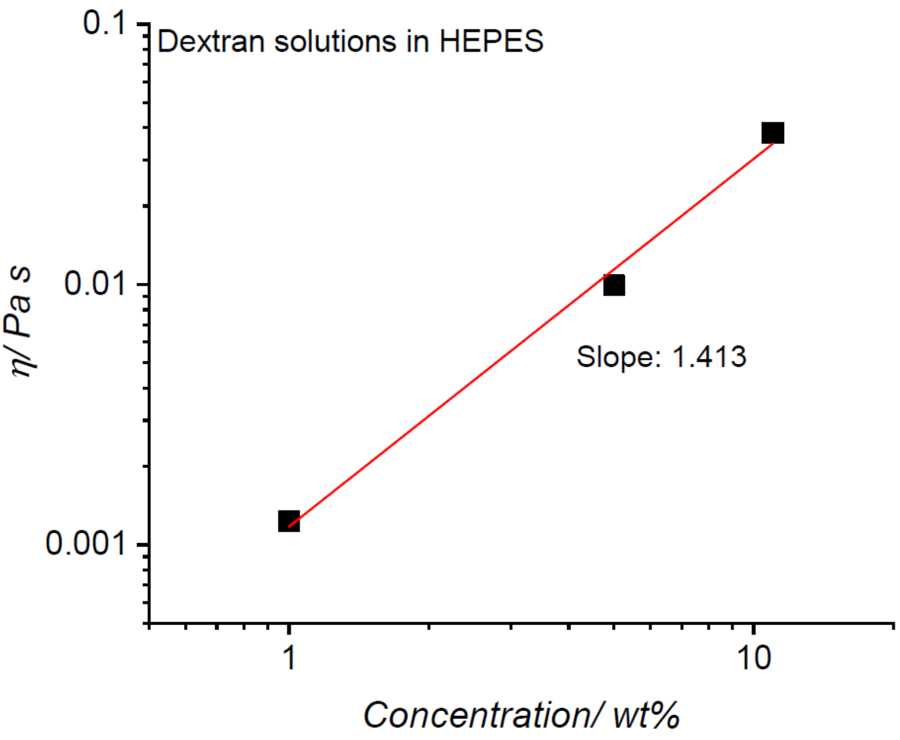

**Figure S2.** The shear viscosity ($\eta$) versus concentration plot in log-log scale for solutions of D[1], D[5] and D[11]. The resultant tangent to the curve obtained by linear fitting showed a slope of 1.4. The same value was reported for dextran with a molecular weight of $2\times10^6$ by Tirtaatmadja, et al. (Tirtaatmadja, Dunstan, & Boger, 2001). This indicates that the concentrations of dextran used in this study were below the critical concentration where a significant change to the shear viscosity has been observed as a result of an increase in dextran concentration shifting the slope to values of around 4 (Tirtaatmadja, et al., 2001). When below the critical concentration, a compact branched configuration with long side-chain in the branches was suggested for dextran.

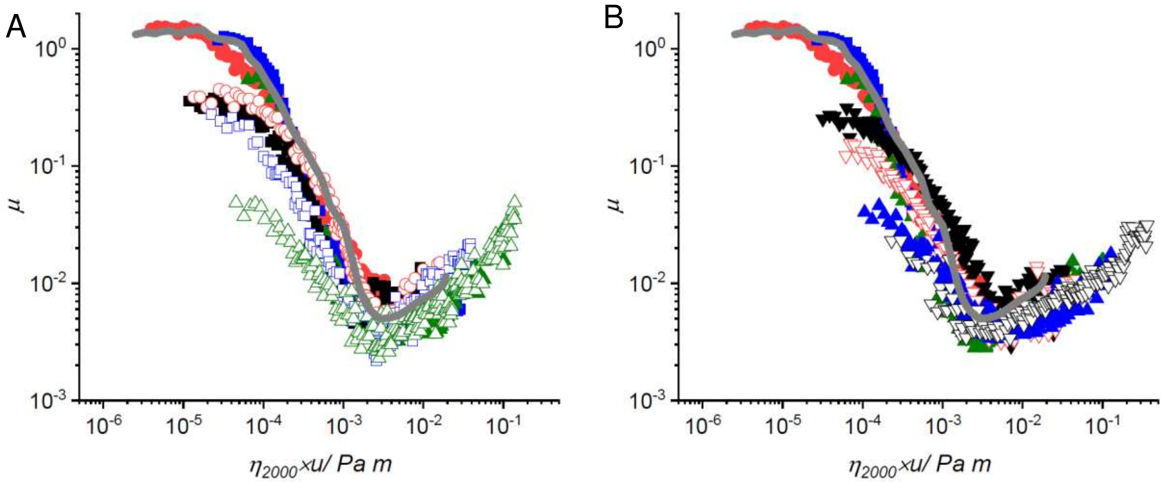

**Figure S3**. Friction coefficient ($\mu$) *versus* product of the high-shear viscosity (at 2000 $s^{-1}$) multiplied by the entrainment speed ($\eta_{2000} \times u$) for biopolymer solutions D[1] (●), D[5] (■), D[11] (▲) and W[5] (■) and mixtures of dextran and whey protein D[1] + W[5] (○), D[5] + W[5] (□), D[11] + W[5] (△). (B) $\mu$ *versus* $\eta_{2000} \times u$ for biopolymer solutions D[1] (●), D[5] (■), D[11] (▲) and the microgel systems WPM (▼), WPM + D[1] (▽), WPM + D[5] (▲), WPM + D[11]. The '*master*' curve for a typical Newtonian fluid is shown in grey line. Means are calculated based on readings on at least triplicate samples (n ≥ 3). The tests were conducted at 37 °C using MTM 2 on three separate PDMS tribopairs and lubricant samples. Note that the viscosity-shear rate curves for WPM + D[5] and WPM + D[11] did not reach a plateau in the flow measurements and shown for comparison purposes.

## References

Tirtaatmadja, V., Dunstan, D. E., & Boger, D. V. (2001). Rheology of dextran solutions. *Journal of Non-Newtonian Fluid Mechanics, 97*(2), 295-301.